Spring 2012

A FM-CW microwave radar for rainfall applications

Matthew James Kemp
University of Iowa

A FM-CW MICROWAVE RADAR

FOR RAINFALL APPLICATIONS

by

Matthew James Kemp

A thesis submitted in partial fulfillment
of the requirements for the Master of
Science degree in Electrical and Computer Engineering
in the Graduate College of
The University of Iowa

May 2012

Thesis Supervisor: Associate Professor Anton Kruger

Graduate College
The University of Iowa
Iowa City, Iowa

CERTIFICATE OF APPROVAL

_____

MASTER'S THESIS

_____

This is to certify that the Master's thesis of

Matthew James Kemp

has been approved by the Examining Committee
for the thesis requirement for the Master of Science
degree in Electrical and Computer Engineering at the May 2012 graduation.

Thesis Committee: _____
Anton Kruger, Thesis Supervisor

_____
David Andersen

_____
Witold Krajewski

To my Family & Friends

ACKNOWLEDGMENTS

I would like to thank my committee members for serving on my committee. I would like to thank all of my colleagues at IIHR and the Iowa Flood Center for their support, especially Dr. Jim Niemeier for his help on debugging of code and procuring of parts, and Devin Wagner for fabricating the prototype boards. I would also like to thank the Iowa Flood Center for their financial support throughout this project. Finally, I would like to thank my advisor, Dr. Anton Kruger, for his continuous support and guidance. Without the discussions and brainstorming sessions we had this work would not have been possible.

TABLE OF CONTENTS

LIST OF TABLES

LIST OF FIGURES

CHAPTER I

INTRODUCTION

The concept of an all-electronic rain gauge was proposed and studied at The University of Iowa, more specifically IIHR-Hydroscience and Engineering (IIHR) and the Iowa Flood Center (IFC) (Mansheim, Niemeir, & Kruger, 2008). They used continuous-wave (CW) radar techniques that measure the Doppler shift created by falling rain drops. The Doppler shift created by the rain drops is directly proportional to their terminal velocity. While the relevance of an all-electronic method of measuring rainfall velocity to researchers and scientists will be described briefly in this chapter, the rest of the thesis is dedicated to the development of a microwave rain gauge sensor for hydrologists.

Motivation

There are several advantages of using an electronic technique to measure the rainfall, rather than the more common method of tipping buckets. A typical tipping bucket rain gauge is shown in Figure 1. A few of these advantages include the lower maintenance associated with an all-electronic rain gauge. Animals making nests in the funnel portion of the tipping bucket and random debris; such as leaves becoming lodged in the funnel, are some of the problems which occur with tipping bucket range gauges. When these problems occur, the data associated with the affected tipping bucket rain gauges are inaccurate and human intervention is required to remove the animal nests and/or debris from the tipping bucket funnels. These issues will not plague an all-electronic rain gauge. For best operation, tipping bucket rain gauges must be calibrated and periodically recalibrated to ensure they remain within specification while collecting data. For example, researchers at The University of Iowa's IIHR-Hydroscience and Engineering calibrate their rain network gauges at least once per year. With an all-electronic rain gauge, the calibration process is a onetime process. Once placed in the

field, observations of temperature and angle of operation can be used to offset biases created by these two artifacts, as their importance will be discussed in later sections. For proper operation, tipping bucket rain gauges must be installed level to avoid biasing one bucket over the other. Even with careful initial installation, one must continually check if the buckets are level—the soil bulges, sinks, and shifts as it saturates, freezes and thaws.

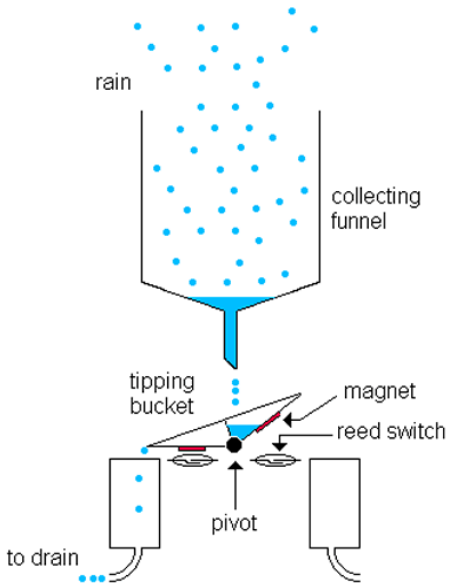

Figure 1. Typical tipping bucket rain gauge setup. The collecting funnel collects rain drops and funnels these drops into the tipping bucket. When the tipping bucket reaches the required threshold (i.e. 1/100" of rain), the tipping bucket swings down and the magnet contacts the reed switch to signify a tip has occurred.

The advantages provided by an all-electronic rain gauge inspired researchers at IIHR investigate a system composed of a commercial agricultural vehicle speedometer that uses Doppler shift techniques (Mansheim, Kruger, Niemeir, & Brysiewicz, 2010). They attached the sensor to a post, and recorded the Doppler shift frequencies generated by falling raindrops. Their sensor was co-located with a well-maintained tipping bucket rain gauge. Figure 2 depicts their experimental setup.

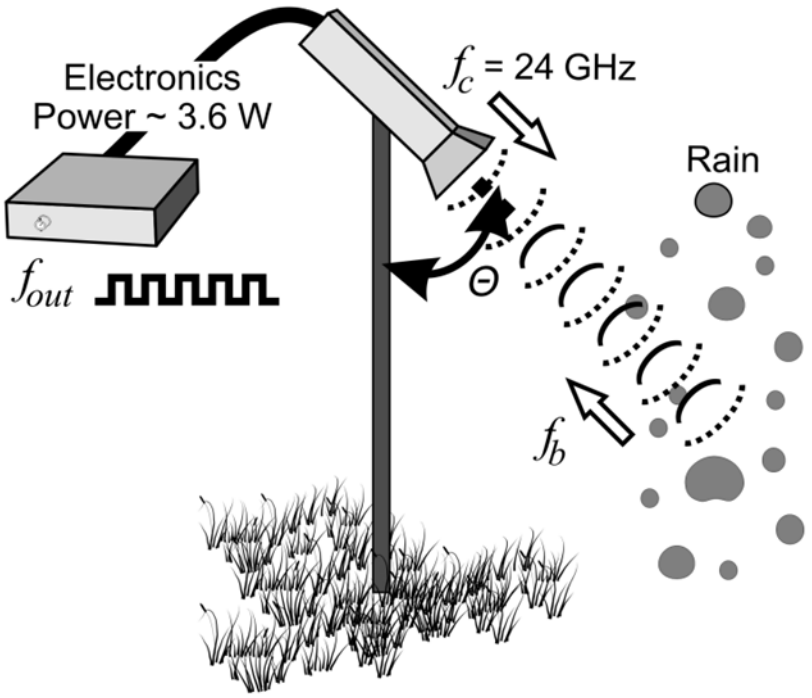

Figure 2. System used by Mansheim et al. (2010) to validate the proposed system by Mansheim et al. (2008). This system used a DICKEY-john Radar I mounted to a post. The sensor's output was sent to electronics for data conversion and logging. (From Mansheim et al., 2010)

The speedometer used by the IIHR researchers uses low power microwaves and measures the Doppler shift of objects in its field of view. The sensor operates as a CW radar. This means that the radar outputs an electromagnetic wave at a constant frequency and constant amplitude. CW is well understood and well-suited for the application of determining rainfall rates (Mansheim et al., 2008).

To better understand the complexity behind outputting relevant information from a CW radar to the end user, a commercial device was torn down. Figure 3 shows the innards of a DICKEY-john Radar III. This particular device is different from the model used by the IIHR researchers as that model has been discontinued by the manufacturer. The current model is no longer sensitive enough to detect rain drops and provides further motivation to develop a low cost, high dynamic range CW radar rain gauge.

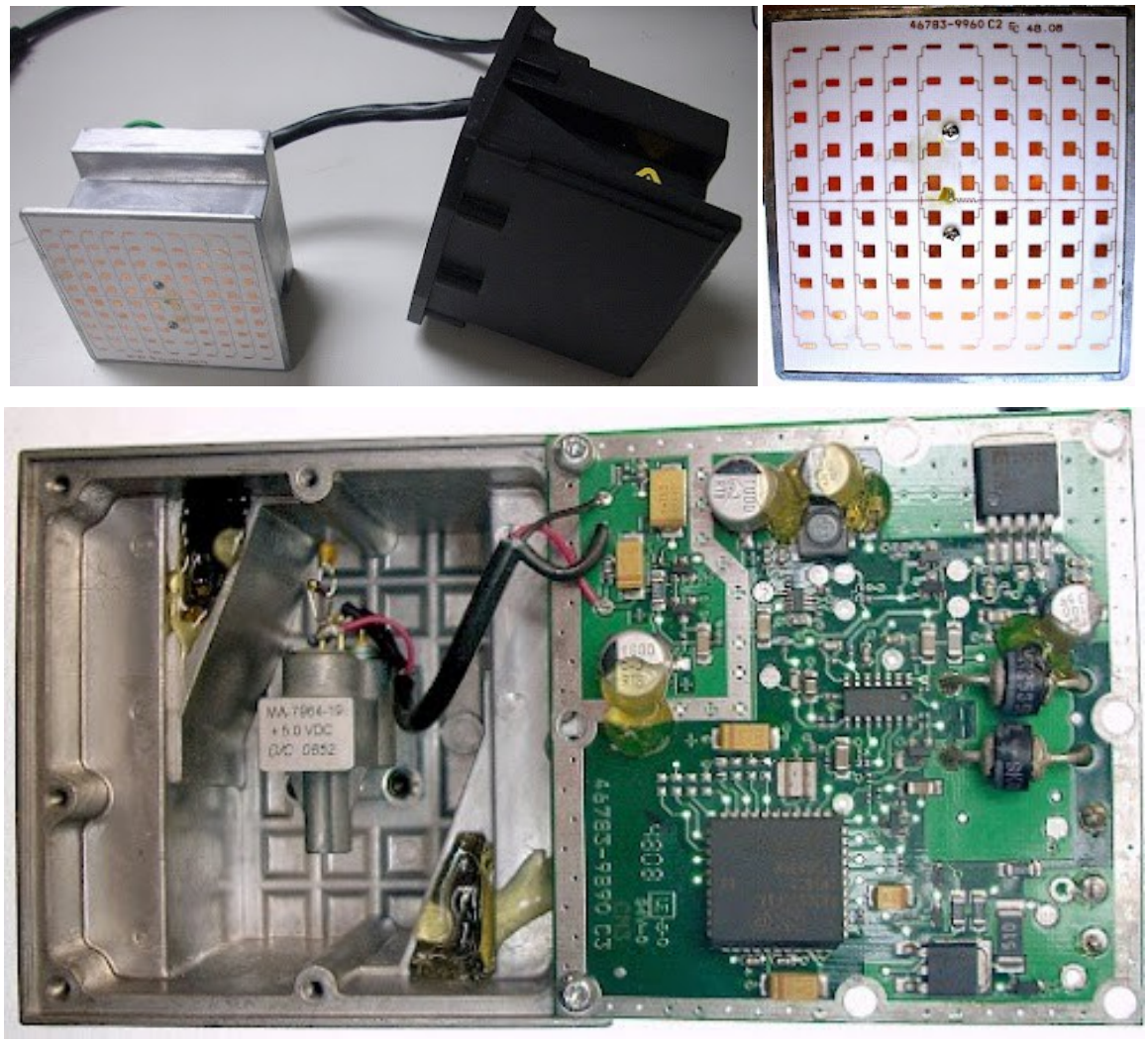

Figure 3. Images of DICKEY-john Radar III. On the top left is a tear down of the water tight packaging used for mounting the device and protecting the electronics from harsh environments. On the top right is the antenna used by the DICKEY-john Radar III, it is a patch array antenna. On the bottom is a tear down of the radar housing. The PCB provides power to the radar and the radar outputs a signal to the PCB. The PCB includes multiple ICs including an 8-bit microcontroller and quad op-amp IC.

Requirements for an All-Electronic Rain Gauge

Although the method proposed by Mansheim et al. (2010) was successful, it did have limitations in the data provided to researchers, as it only provided the frequency of the Doppler shift of the rain drops. Another valuable piece of information that researchers and hydrologists are interested in is the Received Signal Strength (RSS).

The RSS of the signal is valuable as it provides information about a droplet's size and the distance from the radar. This is due to the fact that a large droplet produces a greater RSS than a small droplet falling the same distance from the radar. A similar relationship holds true for the distance a droplet falls away from the radar. The further away a droplet falls, the RSS decreases, while the closer a droplet falls, the RSS increases. The RSS versus distance relationship is examined further in Chapter III.

Other important data are the ambient temperature of the sensor and the angle of operation of the sensor. The ambient temperature of the sensor is needed to account for a small but noticeable temperature dependence of the Doppler shift frequency (Mansheim et al., 2010). Providing the angle of operation of the sensor will help with the initial install. It also provides valuable information for converting the output frequency of the sensor into velocity measurements; this is due to the fact that the frequency to velocity conversion is dependent on the angle of operation.

Besides the desired outputs, a requirement is that the sensor should operate over a range of -5 to 55 ℃. The device should be battery operable as to allow for remote deployment. The device should include an embedded processor to provide a serial interface so that data can be collected without additional interface electronics. The device should also be able to collect data on a range of rain drops (0.5 to 5 mm).

Electronic Methods for Measuring Rainfall

There are many methods for measuring rain fall. One can classify some of these methods as electronic. Three such techniques are the two-dimensional video disdrometer

(2DVD), the Joss-Waldvogel disdrometer and the Pludix disdrometer (Kruger & Witold, 2002).

The 2DVD uses white light sources to create light sheets, which are then projected onto line-scan cameras. The light sheets are rather bright and a particle that passes through the light sheet cast shadows on the photodetectors. To determine if a pixel is lit or obscured, the photodetector signals are compared to a threshold. By determining which pixels are obscured, the physical shape of the hydrometer that obscured the light sheet can be recreated. In principle, using two orthogonal projections, a three-dimensional reconstruction of the hydrometer can be created. The shape information allows computation of the hydrometer's volume and diameter. With this information, the average rain rate can be calculated for a given period.

The Joss-Waldvogel is commonly referred to as an impact disdrometer. As the name suggests, the method of measuring rainfall is done by measuring the impact of a rain drop. This is accomplished by transforming the mechanical momentum of an impacting droplet into an electric pulse (DISTROMET LTD). The amplitude of the pulse is roughly proportional to the mechanical momentum. The mechanical momentum of a droplet is directly related to the size of the droplet. With this information, the average rainfall rate for a given period can be calculated.

The PLUDIX disdrometer is similar to what Mansheim et al. (2010) demonstrated in that the Doppler effect is used to measure droplet velocities. These velocities are then manipulated into drop sizes that will allow one to formulate the average rainfall rate. The PLUDIX is also similar to the efforts put forth here in this thesis (Caracciolo, Natali, Prodi, & Tagliavini, 2002).

A drawback of the 2DVD and Joss-Waldvogel methods is that they require calibration; the 2DVD requires rather careful calibration, while the PLUDIX seems to be a closed system with minimal information available into its inner workings. An ideal solution would be one in which the system could be an open source system that can be

deployed without the need for calibration or one that could monitor its error and be fixed in post-processing of data.

Sensor Block Diagram

The solution will continue on the work of Mansheim et al. (2010) by producing a microwave rain gauge sensor that addresses the limitations the system had due to the use of a commercial product. The microwave rain gauge sensor's high level block diagram is shown below in Figure 4. The system consists of three sensors, a temperature sensor, an inclinometer and a Doppler sensor. The temperature sensor and inclinometer provide digital outputs and will be fed directly into an embedded processor for interpretation. The Doppler sensor's output will need to pass through an analog signal processing chain for filtering and amplification before terminating in an embedded processor for interpretation.

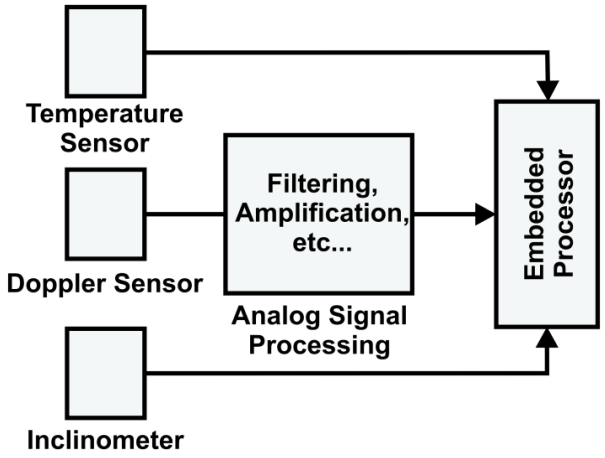

Figure 4. High level block diagram of a microwave rain gauge sensor. The rain gauge consists of three sensors which are a Doppler sensor, temperature sensor and an inclinometer. The Doppler sensor's output is fed into an analog signal processing chain. The outputs of the analog signal processing chain, temperature sensor and inclinometer are terminated at an embedded processor for interpretation. The embedded processor provides data storage and serial interfacing to collect data.

CHAPTER II

BACKGROUND

In this chapter, relevant background information about radars and rainfall is introduced, as well as some information regarding electrical noise. This includes pertinent information about radars such as Doppler effect, received signal strength with relevant equations, significance of antennas, radio spectrum bands, near field vs. far field and different scattering regions. Also included are rainfall properties which are relevant in the design of a microwave rain gauge; such as, rain drop size distribution, droplet shape vs. droplet size and terminal velocity vs. droplet size.

Radar Properties

Doppler Effect

A radar operating in frequency modulated continuous wave, FM-CW, mode provides continuous information. As stated before, the radar will output a constant amplitude, constant frequency continuous wave. When the wave interacts with a target, a certain amount of the wave is reflected and transmitted back to the radar. Figure 5 depicts the process of electromagnetic waves interacting with an object. The reflected wave will demonstrate slightly different characteristics than the original wave. For instance, if the target the original wave reflected off of was moving, the reflected wave will have a different frequency than the original wave. This frequency difference is due to the Doppler effect (Halliday, Resnick, & Walker, 2008). The equation used to determine the Doppler effect is as follows:

$$f_{\mathrm{D}} = V_{\mathrm{Target}} \cos(\theta) \frac{2f_{\mathrm{c}}}{c}$$

where f_{D} is the Doppler frequency, V_{Target} is the velocity of the target being measured, θ is the angle of operation shown in Figure 2, f_{c} is the carrier frequency of the Doppler

sensor and c is the speed of light (Mansheim et al., 2010). Using the phenomena of the Doppler effect, one can calculate the velocity of a moving target by rearranging the above equation for V_{Target}so that

$$V_{\text{Target}} = 2\frac{f_{\text{c}}}{c \times f_{\text{D}}}\cos(\theta)$$

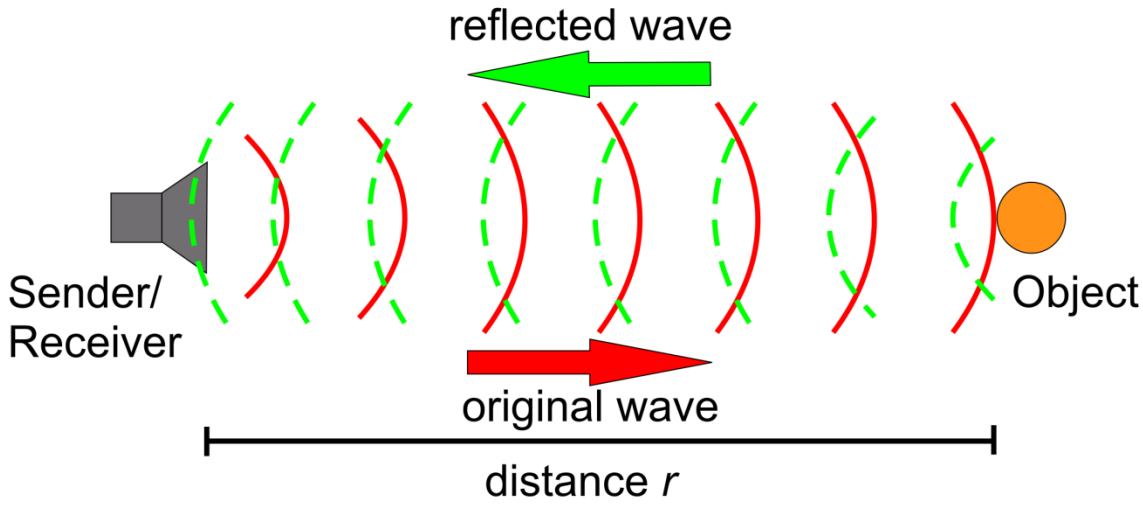

Figure 5. Depiction of a FM-CW radar operating while interacting with a target. The original wave produced by the radar is reflected off of the target and propagates back to the radar. Using the reflected wave's frequency and the original wave's frequency one can determine the velocity of the target by using Doppler shift principals.

Devices have been built that directly output the Doppler frequency and eliminates the need to personally create a processing chain to determine the Doppler frequency. The devices use a method described in Figure 6. The basic idea is that a radar outputs an electromagnetic wave at a specific carrier frequency and the returning wave has a frequency shift that is related to Doppler effect. This returning wave is mixed with the original carrier frequency wave and the carrier frequency is removed from the returning

wave, leaving behind only the frequency shift or Doppler frequency (Mansheim et al., 2010). These devices are commonly referred to as Doppler sensors.

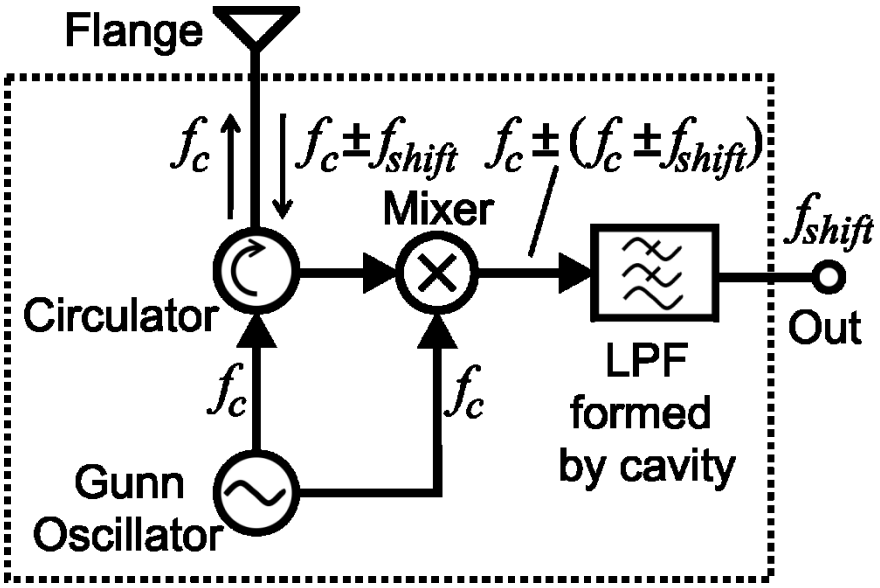

Figure 6. The methodology used by the CW Doppler sensor. An electromagnetic wave is produced at the specified carrier frequency and the reflected wave returns with a frequency shift directly proportional to the Doppler effect. The mixer produces sum and difference frequencies based on the reflected frequency and the carrier frequency. The cavity filters out the summed frequency and leaves behind the difference frequency which is the Doppler frequency. The Doppler frequency is then output from the sensor. (From Mansheim et al., 2010)

Received Signal Strength

As mentioned before, the RSS is valuable in the retrieval of information pertaining to target size and distance. The reason for changes in RSS associated with the distance the waves travel is due to the inherent attribute of electromagnetic waves and how they propagate through free space. As can be seen in Figure 5, the electromagnetic waves propagate radially from their source. This causes the power transmitted to disperse by the surface area the waves cover. The equation that describes this is the

power density equation, which states that the power density of a wave is proportional to the transmitted power divided by the surface area; where the surface area is the surface area of a sphere in the case of radar. The mathematical formula is as follows:

$$S = \frac{p_t}{4\pi r^2}$$

where S is the power density, p_t is the power transmitted and r is the distance traveled (Rinehart, 2004).

An object's size is another variable that directly affects the RSS. This is due to the fact that a larger object will reflect more of the electromagnetic waves than a smaller object. This phenomena is called backscattering and it is directly related to the cross sectional area of the object (Rinehart, 2004). To better understand this, if the object in Figure 5 is replaced with a smaller or larger sphere, the expected initial reflected wave will be smaller or larger, respectively.

These two attributes of target distance and target backscattering cross sectional area are captured by the radar equation for a point target. The radar equation is:

$$p_r = \frac{p_t g^2 \lambda^2 \sigma}{64\pi^3 r^4}$$

where p_t is the power transmitted, g is the gain of the antenna, λ is the wavelength of the radar, σ is backscattering cross-sectional area of the target and r is the distance from the target to the radar (Rinehart, 2004). One may notice a slight difference in the relationship of distance from the power density equation to the radar equation, this is due to the fact that the power density equation is assuming one directional flow of the waves and does not take into account the physics behind the reflected wave and its propagation.

Antennas

The main purpose of an antenna is to transmit or receive electromagnetic waves (Balanis, 2005). Although this is their main purpose, the construction of an antenna can play a significant role in how the electromagnetic waves propagate in free space and the

power of these transmitted waves. The significance of antennas is captured in the radar equation by the variable g, which is the antenna gain. The gain of an antenna is in reference to its ability as a transmitter to convert input power to radio waves or as a receiver to convert radio waves to electrical power. For example, the gain of a short dipole antenna is ~1.76 dBi and the gain of the world's largest parabolic antenna is ~70 dBi; while the gain of the horn antenna discussed in Chapter III is ~20 dBi.

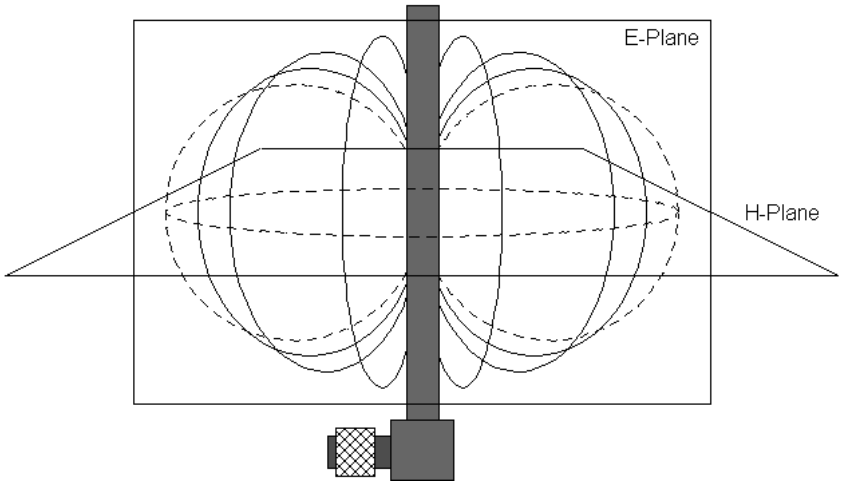

Figure 7. Radar propagation field of an omnidirectional antenna. As can be seen here, the field propagates in all directions.

Antennas tend to fall into one of two categories, omnidirectional or directional (Balanis, 2005). An omnidirectional antenna, for the most part, receives or radiates in all directions. This is most often implemented when the location of other nodes is unknown or arbitrary so the electromagnetic waves will cover a large area. Omnidirectional antennas are frequently used in low frequency applications because directional antennas can become very large at low frequencies as their characteristics are related to the wavelength of the electromagnetic waves. Applications that make use of the properties of omnidirectional antennas are mobile devices and FM radios.

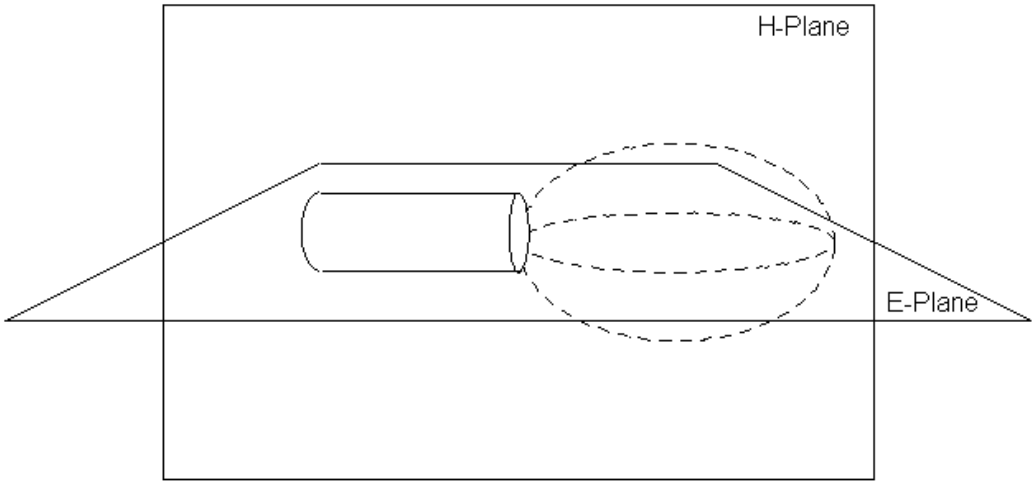

Figure 8. Radar propagation field of a directional antenna. As can be seen here, the field propagates in a specific direction.

Directional antennas, as their name suggests, radiate or receive electromagnetic waves in a particular direction (Balanis, 2005). Due to directing the electromagnetic waves in one direction, the energy in the particular direction is increased, allowing for further propagation of the waves. A side effect of directing the waves is that the beam width of the waves is decreased. Due to these characteristics of directional antennas, they are best suited for applications where the location of the node in which it is sending to or receiving from is known. Applications that make use of the properties of directional antennas are radar guns and automatic door openers.

Radio Spectrum

The radio spectrum is in reference to the electromagnetic spectrum corresponding to radio frequencies. They are generally thought of as frequencies that are lower than 300 GHz. A band is a section of the radio spectrum and, for purposes of this document, the IEEE defined spectrum will be used. The spectrum and band segmentation can be found in Appendix A. The relevant bands for the rest of this paper are the X-band

(10 GHz), K-band (24 GHz) and Ka-band (35 GHz) (IEEE Aerospace & Electronic Systems Society, 2003).

Near Field vs. Far Field

All radars have two main fields through which an object can pass, the near field and the far field (Skolnik, 2003). There is also a transition zone where the near field effects begin to taper off and the far field effects tend to dominate. The reason for the need of different fields is due to the fact that certain characteristics of an electromagnetic field change with the distance from the source of the electromagnetic field. Not surprisingly, the near field is in close proximity to the source and the far field is essentially everything that is not in the near field or transition zone.

Although the exact transition from near field to far field is disputed by physicists, a few general rules are well accepted. For short antennas, where the antenna's largest dimension is shorter than half the wavelength of the radiation they emit, the near field is thought to be the distance less than one wavelength away from the source (Skolnik, 2003). The transition zone is from one wavelength to two wavelengths and the space beyond two wavelengths is the far field. A graphical description of this can be seen in Figure 9.

For long antennas, where the antenna's largest dimension is longer than half the wavelength of the radiation they emit, these rules are no longer valid. Instead, the guidelines used for long antennas are the near field only effects ends at

$$r = 0.62\sqrt{D^3/\lambda}$$

where r is the distance, D is the largest dimension of the antenna and λ is the wavelength of the electromagnetic waves. Far field only effects begin at distances greater than

$$r = \frac{2D^2}{\lambda}$$

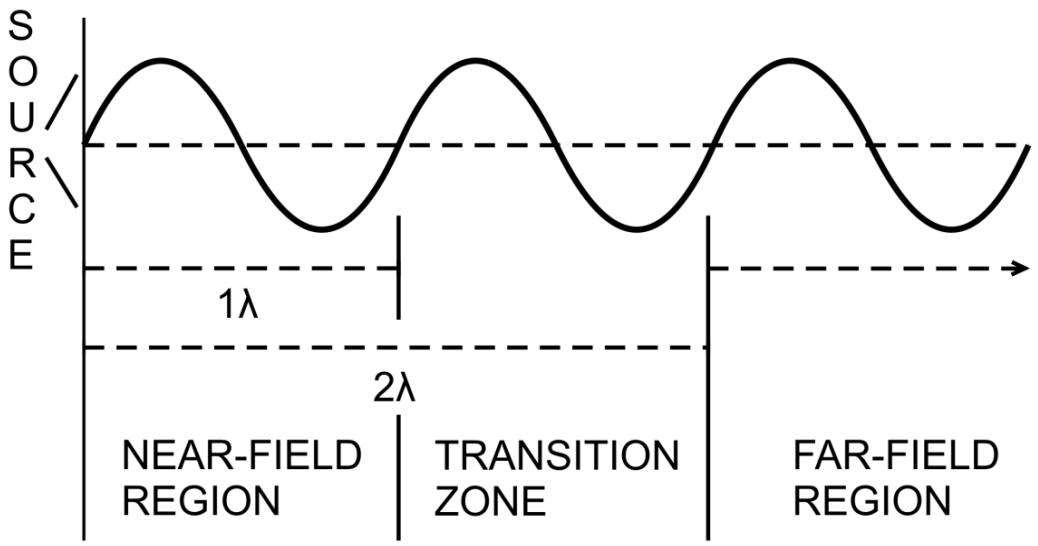

Figure 9. Graphical representation of the near and far field regions of a short antenna.

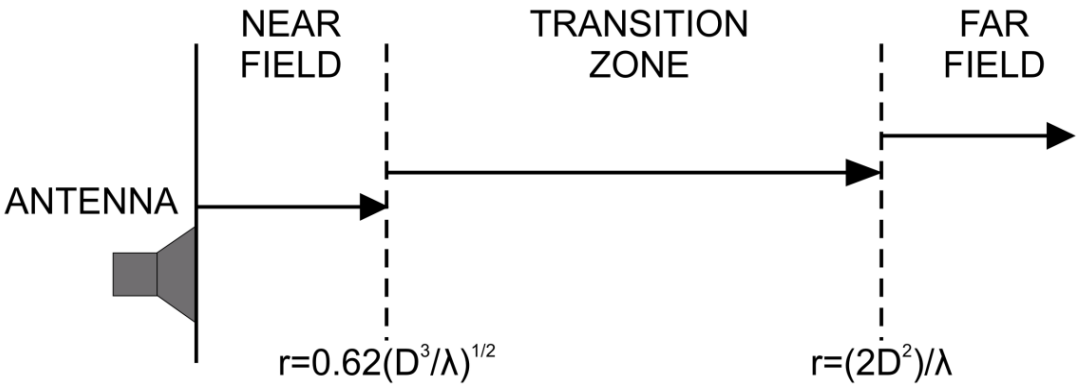

Figure 10. Graphical representation of the near and far field regions of a long antenna.

where r is the distance, D is the largest dimension of the antenna and λ is the wavelength of the electromagnetic waves (Skolnik, 2003). A graphical description of this can be seen in Figure 10.

Scattering Regions

As previously mentioned, the backscattering cross sectional area of a target is directly related to the power received back at the source of the radar. However, this cross sectional area is not always directly related to the physical dimensions of the target. Targets fall into three regions with respect to their cross sectional area, namely the Rayleigh region, the Mie region and the optical region (Skolnik, 2003).

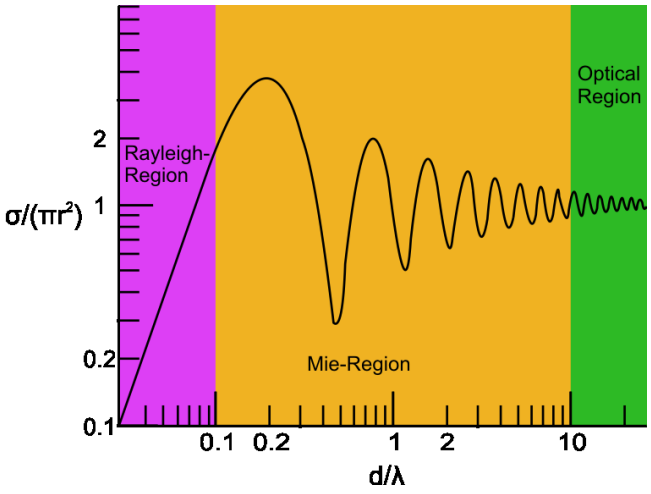

Figure 11. Plot of different scattering regions showing the radar cross sectional area observed in relation to the physical cross sectional area of a spherical target for spherical targets' diameters in relation to wavelength.

The appropriate region is determined by the object's diameter in relation to the wavelength of the radar. A spherical object that is ten times smaller than the wavelength is in the Rayleigh region, a spherical object that is similar in size to the wavelength is in the Mie region and a spherical object that is ten times larger than the wavelength is in the

optical region. These different regions all treat a target's cross sectional area differently. In the Rayleigh region, the spherical object's cross sectional area is seen as smaller than the geometric cross sectional area. In the Mie region, the spherical object's cross sectional area tends to oscillate back and forth but tends to be larger than the geometric cross sectional area. In the optical region, the spherical object's cross sectional area tends to be true to the geometric cross sectional area. A plot of these different regions is shown in Figure 11.

Rainfall Properties

Rain Drop Size Distribution

With the backscattering cross sectional area of a target being one of the controlling factors of the radar equation, it would be beneficial to better understand the expected target sizes to be encountered by the Doppler sensor module. Fortunately, scientists have studied rainfall drop size distribution properties for many years. Krajewski et al. (2006) is a well-accepted source for determining the possible drop size distribution that can be experienced in nature.

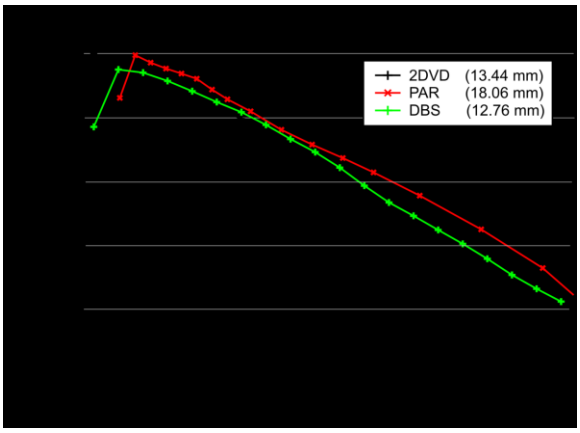

Figure 12. Drop size distribution as measured by multiple disdrometers at the Iowa City Municipal Airport. (From Krajewski, et al., 2006)

However, the distribution of the droplets occurrence in nature is not evenly distributed for each droplet size. The drop size distribution is often modeled as a lognormal distribution with the vast majority of the drops being between 0.5 to 1 mm, as shown in Figure 12. For the end system to be practical, it must be able to handle a large majority of these droplet sizes and is the reason the requirement for detection of 0.5 to 5 mm drops is imposed.

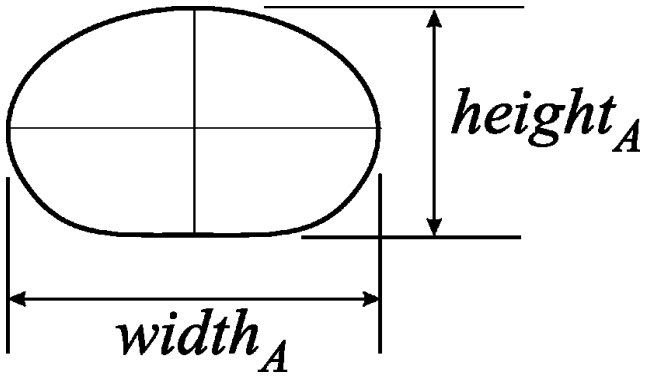

Figure 13. Graphic depicting a more realistic model of droplet shape for drops greater than 2 mm in diameter. Droplets less than 2 mm in diameter tend to be more spherical. (From Krajewski, et al., 2006)

Droplet Shape vs. Droplet Size

A common misconception is that all rain drops fall in a tear drop shape. However, in reality, small drops, those measuring 2 mm or less in diameter, are spherical. As the drop size increases, the drops become oblate. Large drops oscillate and can have different shapes (Krajewski, et al., 2006). Figure 13 is a good representation of true droplet shape for droplets larger than 2 mm.

Terminal Velocity vs. Droplet Size

The terminal velocity of different size droplets is also important to a designer of a microwave rain gauge, as Doppler shift frequency is directly related to the terminal

velocity of a droplet (Atlas, Srivastava, & Sekhon, 1973). A well accepted equation used to model the relationship of terminal velocity vs. droplet size was developed by Atlas et al. which states

$$v = 9.65 - 10.3e^{-0.6D}$$

where v is the velocity in m/s and D is the diameter of the droplet in mm. A plot representing this equation is shown below in Figure 14. A numerical set of data points are shown in Table 1 for this equation.

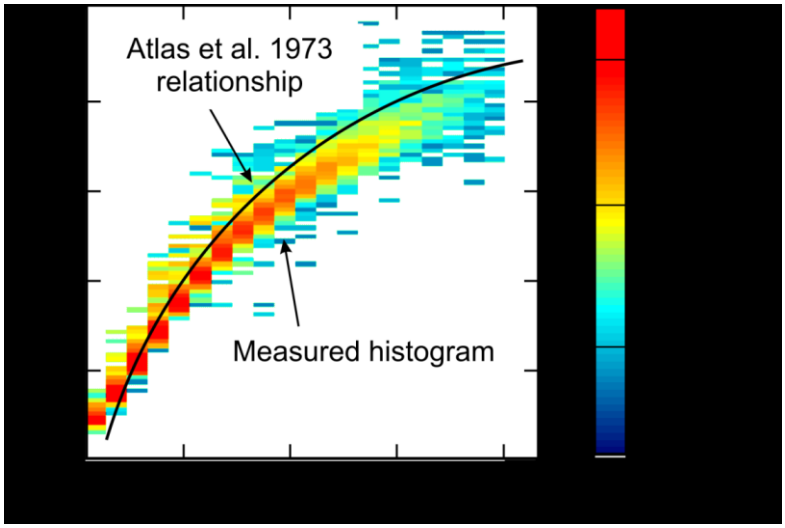

Figure 14. Plot of fall velocity vs. drop size diameter. The plot includes the theoretical equation of fall speed and the observed fall speed determined using disdrometers. (From Krajewski, et al., 2006)

Table 1. Velocity values calculated using Atlas et al. (1973) relationship

Drop Size (mm)	**Velocity (m/s)**
0.5	2
1	4
3	8
5	9.1

Electrical Noise

Noise can be classified as one of two types of noise, external noise or internal noise (Franco, 2002). The two most common types of noise are white noise and $1/f$ noise. White noise is directly proportional to the bandwidth of the signals to be used because it's fairly constant across the entire spectrum. The amount of white noise that will affect circuitry can be determined by using the following equations:

$$E_n = e_{NW}\sqrt{f_H - f_L}$$

$$I_n = i_{NW}\sqrt{f_H - f_L}$$

where E_n is the voltage noise from white noise, e_{NW} is the spectral voltage noise density, f_H is the high frequency of the spectrum to be analyzed, f_L is the low frequency of the spectrum to be analyzed, I_n is the current noise from white noise and i_{NW} is the spectral current noise density. $1/f$ noise can be specified by the following equations:

$$E_n = K_V\sqrt{\ln\left({f_H}/{f_L}\right)}$$

$$I_n = K_I\sqrt{\ln\left({f_H}/{f_L}\right)}$$

where K_V is the voltage noise constant related to $1/f$ noise and K_i is the current noise constant related to $1/f$ noise. As can be seen here, the noise produced by white noise and $1/f$ noise is proportional to the bandwidth of the frequencies. Therefore, to reduce the amount of noise in the system, it is advantageous to reduce the bandwidth as much as possible.

CHAPTER III

DOPPLER SENSORS AND THEIR SIGNAL SIGNATURE

In this chapter, an investigation of Doppler sensor modules will be documented. This includes the effects different modules will have on the final design and the signal signature from the output of these modules.

Doppler Sensor Modules

The selection of the Doppler sensor module plays a significant role in the circuitry that follows; for this reason several modules were investigated. These modules covered different carrier frequencies, different oscillator construction and different antennas. The biggest concerns were achieving a high S/N ratio and increasing the minimum Doppler frequency at the output of the module. The Doppler sensor modules that were investigated can be seen in Figure 15. Table 2 summarizes the characteristics of the different modules.

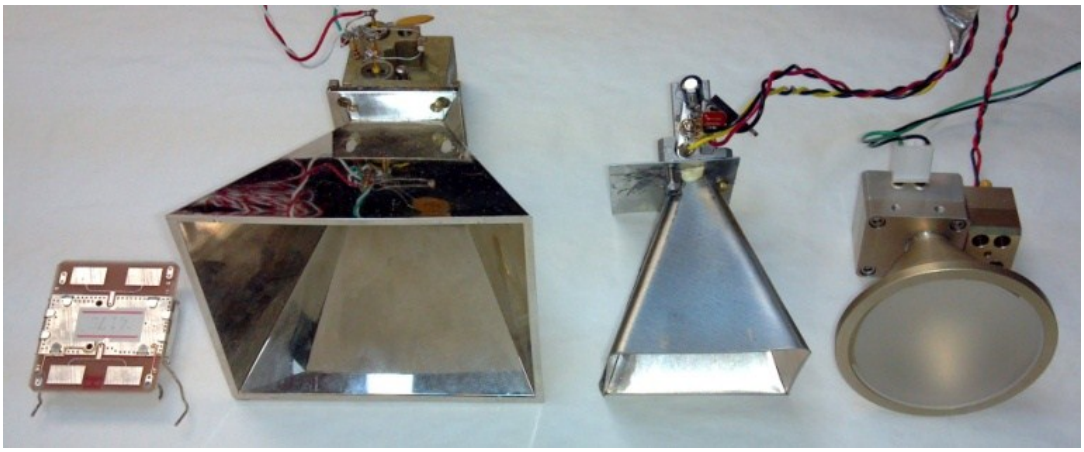

Figure 15. Collection of Doppler sensor modules explored for use in the rain gauge sensor. From left to right, X-band dielectric resonantor oscillators with patch array antenna, X-band Gunnplexer with pyramidal horn antenna attached, K-band Gunnplexer with pyramidal horn antenna attached and Ka-band Gunnplexer with lens-corrected horn antenna.

Table 2. Characteristics of the Doppler sensor modules investigated

	X-band DRO (NJR4175)	**X-band Gunn** (MA87728)	**K-band** (NJR4211)	**Ka-band** (SRF-35120610-01)
Center Frequency (GHz)	10.525	10.525	24.15	35.5
Output Power (mW)	20	10	4	10
Operating Voltage (V)	5	8	5	5
Operating Current (mA)	30, typical	200, max	130, max	500, max

Carrier Frequency

The carrier frequencies that were examined were X-band, K-band and Ka-band. The carrier frequency, as explained earlier, directly determines the range of expected Doppler frequencies. Consider, for example, an X-band module operating nominally at f_c = 10.525 GHz. The minimum expected Doppler frequency occurs with small drops with fall speeds on the order of 0.5 m/s. Assuming the sensor is mounted at an angle of 45°, this translates to

$$f_{\mathrm{D}} = V_{\mathrm{Target}} \cos(\theta) \frac{2f_{\mathrm{c}}}{c} = 25 \text{ Hz}$$

A similar calculation shows that the maximum expected f_{D} is 546 Hz. Unfortunately, the radar modules are quite susceptible to pickup of and interference from 60-Hz mains power. Since the vast majority of rain drops are small and have small fall velocities, their corresponding Doppler frequencies are closer to 60 Hz rather than 546 Hz. Filtering to remove 60 Hz interference will also remove the desired Doppler signals.

Table 3. Expected max and min Doppler frequencies

f_c (GHz)	Min f_D (Hz)	Max f_D (Hz)
10.525	25	546
24.15	57	1,253
35.5	84	1,842

Note: The values are based on rain drop fall speeds that range from 0.5 m/s to 11 m/s and an angle $\theta = 45°$.

Thus, it is desirable to use modules that operate at higher frequencies, since this moves the lowest f_D above the 60-Hz interference and one can filter the 60 Hz noise without complex schemes. As shown in Table 3, the Ka-band radar operating at 35.5 GHz is ideal. Higher frequencies may be beneficial, but as carrier frequencies increase, attenuation of the electromagnetic waves increases as well.

Table 4. Scattering region boundaries

f_c (GHz)	Wavelength (mm)	Rayleigh Region (mm)	Mie Region (mm)	Optical Region (mm)
10.525	28.5	0-2.85	2.85-285	285-∞
24.15	12.41	0-1.24	1.24-124	124-∞
35.5	8.44	0-0.84	0.84-84	84-∞

The carrier frequency also controls the boundaries of the scattering regions. Table 4 shows the scattering region boundaries expected for the different carrier frequencies of interest. Clearly, for rain and the microwave frequencies being investigated, scattering is either in the Rayleigh or Mie region.

Oscillator Construction

Two distinct types of radar modules were investigated, namely dielectric resonator oscillators (DRO) based modules and Gunn-diode based modules. Each type of radar has its advantages and disadvantages.

Dielectric Resonator Oscillators

One of the advantages of DROs is that they are compact. Further, DROs' carrier frequencies show less dependence on temperature than Gunn diode modules. However, the DRO modules that were easily obtainable were on PCB substrates, and integrated with patch array antennas. These integral antennas have a wide radiation pattern. Since a high S/N ratio is imperative for the design, and the patch antenna does not allow for the attachment of a high gain directional antenna, this particular DRO module is not well suited for use in the microwave rain gauge.

Gunn diode

Gunn diode modules, sometimes referred to as Gunnplexers, are designed for attachment to a waveguide, making it easy to attach high gain directional antennas; such as horn and cone antennas. The downside of using a Gunnplexer is that the carrier frequency is dependent on the cavity (waveguide) in which it is placed. A waveguide controls the carrier frequency, as the boundary conditions imposed by the physical dimensions of the waveguide set a bound for the lowest frequency that can traverse the waveguide, thus a waveguide acts as a high pass filter for electromagnetic waves. For this reason, manufacturers of Gunnplexers allow their customers to tune the cavity by means of screws or some other mechanism. This way, the cavity can attempt to match the carrier frequency specified by the Gunnplexer manufacturer.

Oftentimes, these cavities are made of some type of metal alloy, which tends to change their physical characteristics over large temperature spectrums. For this reason, the carrier frequency of a Gunnplexer may change from a cold day to a warm day. There

are methods to help combat this issue that try to maintain the cavity at a constant temperature. Since the carrier frequency does alter the Doppler frequency measured, a solution is needed to compensate for this change in carrier frequency (Mansheim, et al., 2010). In order to resolve this issue, a temperature sensor will be placed in close proximity to the Doppler sensor module to monitor the temperature experienced by the module. This way, if during field trials with co-located tipping buckets, the data demonstrates that during colder or warmer temperatures the microwave rain gauge produces a biased result; an algorithm can be devised that accounts for this bias in post-processing as the temperature will be known. For these reasons, the use of a Gunnplexer Doppler sensor module in the design of the microwave rain gauge would be beneficial.

Antenna Design

When attempting to measure small drops from a distance of about 0.5 m, the S/N ratio of a Doppler sensor is low. There are two ways to increase the S/N ratio: reduce the noise by filtering and choosing low noise components, or by increasing the signal. As discussed earlier, a directional antenna can be utilized to boost the signal. This way, the Doppler sensor's output will be amplified as compared to when there is no antenna.

A rather simple yet very effective antenna is a horn antenna. A horn antenna operates similar to how a megaphone amplifies sound, in that the amplification comes from focusing the energy in one direction. Horn antennas are well-understood and easy to design. There are a few different types of horn antennas, two of which are the pyramidal and the conical. In this investigation, the pyramidal horn antenna was used due to the ease of their construction.

A freeware version of a simple design tool was chosen to design the horn antenna. In order for the software to design a pyramidal horn antenna, parameters were needed; the first being the carrier frequency that is to be amplified, the second was the dimensions of the waveguide that the horn antenna will be attached to and, lastly, the gain one wishes

to receive out of the horn antenna as compared to an isotropic antenna. The antenna was designed for the K-band module and can be seen attached to the Doppler sensor module in Figure 15. This particular antenna was designed for a gain of 20.05 dBi and the results of the antenna on the output signal are in the following section in Figure 17. The template for the horn antenna is in Appendix B.

Signal Signature

To begin design work on any circuitry, it is imperative to understand the input and its possible variations. For this reason, an investigation of the Doppler sensor's signal signature was done, as well as, formulating the expected range of signals to be output by the Doppler sensor modules. However, one design consideration can already be made in the removal of the two X-band modules as the minimum Doppler frequency is well below 60 Hz and complex filtering techniques would be undesirable when a simpler solution such as choosing the K- or Ka-band module is viable. Due to module availability, only the K-band module will be discussed in the rest of this thesis, and may be referred to as the Doppler sensor module. The signal signature from a Doppler sensor module is shown below in Figure 16.

The signal in Figure 16 was produced by bandpass filtering (cutoff frequencies of 72 Hz and 1,600 Hz) the output and amplifying the signal by ~1,250. This signal manipulation was necessary in order to produce a signal where the characteristics of the signal signature can be captured by a digital oscilloscope. This particular signature was produced by a ~3 mm diameter water drop passing by the K-band Doppler sensor ~15 cm in front of the antenna. As can be seen in Figure 16, the voltage level is not of constant amplitude as it increases and decreases as it passes in front of the Doppler sensor. This is due to the drop moving closer to the antenna and then farther away.

The frequency of the signal signature is directly proportional to the velocity of a droplet. The equation used to determine this frequency was introduced earlier as the

Doppler frequency equation. Also, it should be noted that when looking at Figure 16, the frequency increases as time progresses. This can be attributed to the fact that the angle the drop is in relation to the radar changes as the drop passes by the radar. This can also be attributed to the fact that the droplet used to produce this signal had not yet reached terminal velocity, as it was dropped only one meter above the radar. Therefore, the droplet was still accelerating and its velocity increasing as it passed in front of the sensor which leads to an increase in frequency as time progressed.

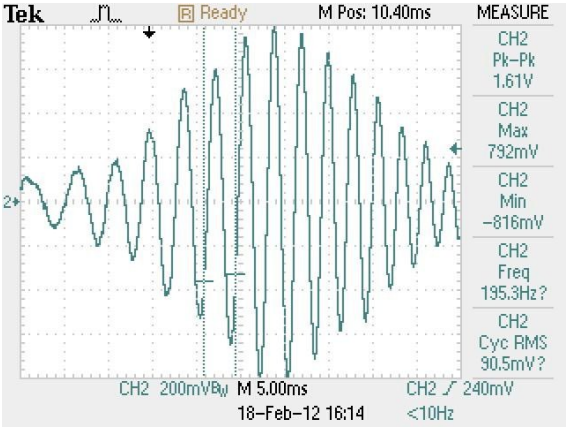

Figure 16. Screen capture of output of Doppler sensor module with carrier frequency of 24.15 GHz, made with a Tektronix TDS 2022B oscilloscope using a 1× probe. The signal was bandpass filtered (cutoff frequencies of 72 Hz and 1,600 Hz) and amplified by ~1,250. The signal is produced by a water drop of ~3 mm in diameter at a distance of ~15 cm from the edge of the Doppler sensor's antenna. The drop in this figure had not reached terminal velocity as it was dropped one meter above the radar.

Since the expected frequency ranges output by the Doppler sensors were already determined in the previous section, the other necessary portion of the input to understand is the dynamic range of the amplitude. Since an antenna will be attached, the effects this will have on the output of the Doppler sensor must be considered, as it will involve more than just increasing the S/N ratio of the Doppler sensor output. The difference between

the non-antenna output and the antenna output of the Doppler sensor can be seen in Table 5 and Figure 17. Using the average values calculated in Table 5 shows that the antenna produces a gain of more than 10 dB.

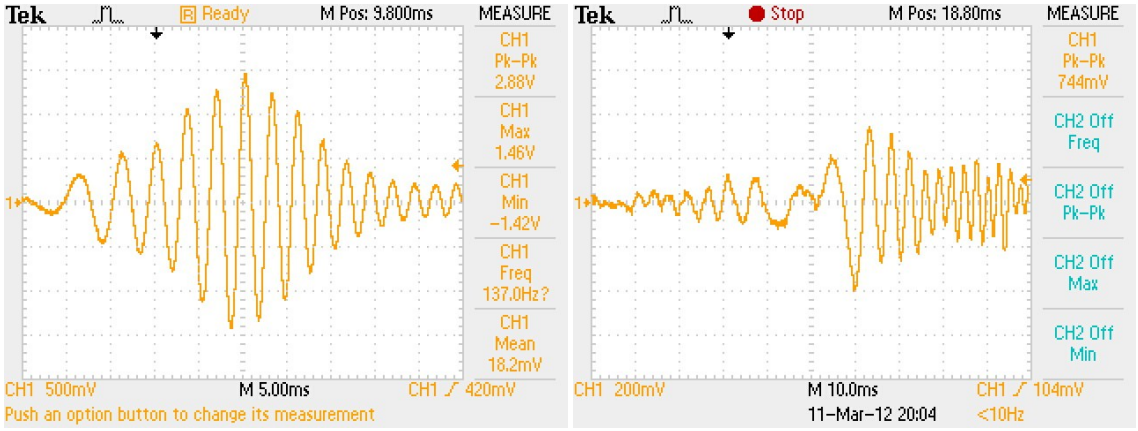

Figure 17. On the left is the output of the Doppler sensor module with the horn antenna attached. On the right is the output of the Doppler sensor module without the horn antenna attached. These images are created from a 3 mm steel ball being dropped ~15 cm away from the Doppler sensor.

Table 5. Pk-Pk output by K-band sensor with and without horn antenna

	Drop 1	**Drop 2**	**Drop 3**	**Drop 4**	**Drop 5**	**Average**
Pk-Pk with Antenna (V)	2.84	2.88	2.58	2.26	2.94	2.7
Pk-Pk without Antenna (V)	0.664	0.88	0.904	0.896	0.744	0.818

Note: These values are amplified by ~1,250 times.

However, as a result of adding an antenna to increase the S/N ratio, the effects of near field and far field must also be considered. The 20.05 dBi antenna produced for the K-band module has a largest dimension of 55 mm, making the antenna attached to the K-

band antenna a long antenna. Therefore, near field effects are present in the region less than

$$r = \frac{2D^2}{\lambda} = \frac{2 \times 55^2}{12.41} = 48.75 \text{ cm.}$$

Since this is a region in which the device will operate, effects of the near field must be accounted for when determining the dynamic range.

Recalling that the power received by the radar is

$$p_r = \frac{p_t g^2 \lambda^2 \sigma}{64\pi^3 r^4}$$

suggests that determining the dynamic range should be fairly easy. For a particular radar, everything is a constant besides σ and r, so that

$$p_r \propto \frac{\sigma}{r^4}.$$

Since power is proportional to the square of voltage, the output voltage of the Doppler sensor will be

$$v_r \propto \frac{\sigma}{r^2}$$

Naïvely, taking the backscattering cross sectional area as proportional to the square of the drop diameter, then

$$v_r \propto \frac{d^2}{r^2}.$$

However, there are two reasons why the power received equation should be modified. First, as was discussed earlier, the radar will be operating in multiple scattering regions and therefore the backscattering cross sectional area will differ by more than just its geometric properties. Secondly, the radar equation implicitly assumes the point target is in the antenna's far field. As discussed earlier, near filed operation is more appropriate to consider. Since the microwave rain gauge operates in multiple scattering regions and operates in the near field of the radar, the final voltage relationship described

above cannot be used. Consequently, a received power relationship was determined experimentally.

Received Signal Model

Figure 18 shows the result for RSS versus target distance, obtained by dropping metal spheres at various distances in front of the Doppler sensor. Figure 19 shows the results for the RSS versus drop diameter. The data show that $v_r \propto 1/r^{1.6}$ model the data reasonably well. The data also show that $v_r \propto d^{1.4}$, where d is the diameter of the target, models the receiver signal versus target diameter well. Combining the experimental results for the distance r from the radar and drop diameter d, results in

$$v_r \propto K \frac{d^{1.4}}{r^{1.6}}$$

where K is some constant that is a function of the Doppler sensor module, such as gain of the antenna, transmitted power, amplification, etc.

Using this information and the expected range for rain drop diameters, the maximum and minimum peak-to-peak (Pk-Pk) voltage expected to be produced by the Doppler sensor can be calculated as can be seen below in Table 6, which shows a 72-dB dynamic range. The data provided in Table 6 are the controlling factors for the analog circuitry for specifications such as the amount of gain possible yet still avoid clipping, as well as the amount of compression needed.

Table 6. Estimated Pk-Pk voltage produced by a Doppler sensor module

Drop Diameter (mm)	**Drop Distance (cm)**	**Sensor Output (Pk-Pk mV)**
5	2.5	46
0.5	60	0.011

Note: Values calculated using power law relationships for the diameter of the drop and distance from the radar and using the Pk-Pk voltage normalized by 1,250 from Figure 16.

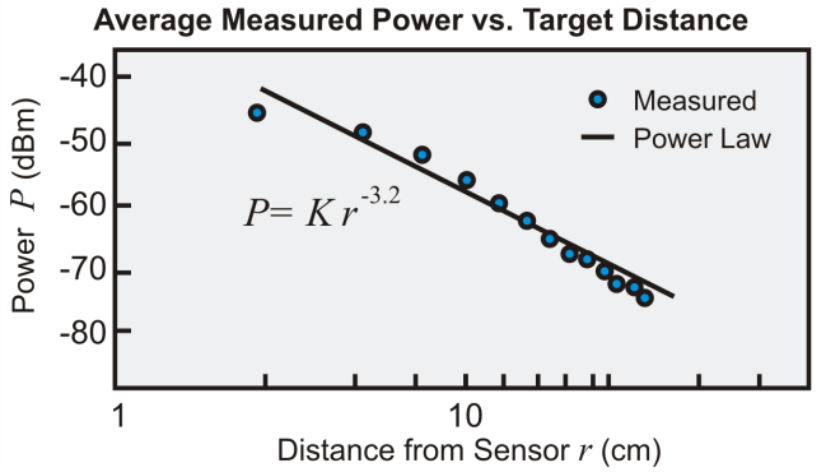

Figure 18. Plot of average power received by the Doppler sensor vs. target distance. The data were collected by dropping metal spheres 3 mm in diameter at set distances from the sensor and averaging the peak power received. The plot suggests that $p_r \propto 1/r^{3.2}$ rather than $p_r \propto 1/r^4$ predicted by the radar equation. Note that $p_r \propto 1/r^{3.2}$corresponds to $v_r \propto 1/r^{1.6}$ for sensor voltage.

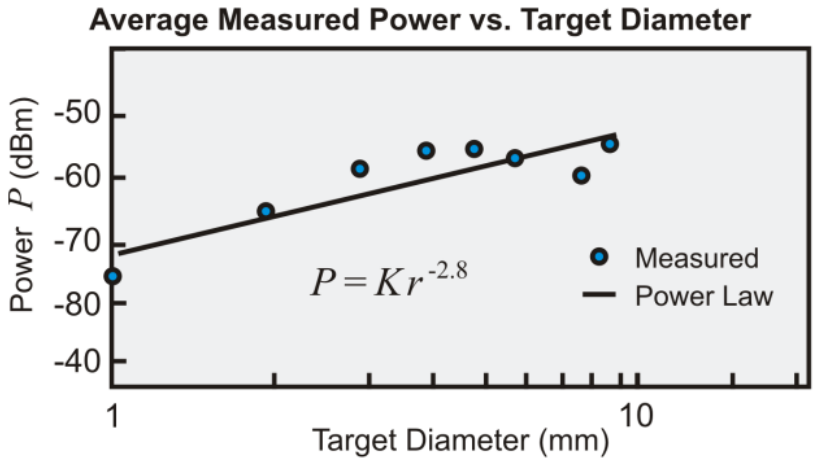

Figure 19. Plot of average power received by the Doppler sensor vs. target size. The data were collected by repeatedly dropping metal spheres of varying size at 15.25 cm from the Doppler sensor and averaging the peak power received. The plot suggests that $p_r \propto d^{2.8}$. Note that $p_r \propto d^{2.8}$ corresponds to $v_r \propto d^{1.4}$ for sensor voltage.

Noise Floor

The noise produced by the Doppler sensor is also of interest, as the noise floor of the sensor will determine the smallest possible RSS that can be recovered. Unfortunately, the data sheets for the Doppler sensor modules do not specify the noise inherent to the sensor. It is also not a straight forward measurement to determine the noise that is output by the Doppler sensor modules, as the tools readily available to determine the noise also have inherent noise, as will be shown.

To determine the noise floor, a few measurements were taken using the Tektronix TDS 2022B digital oscilloscope. The first being the peak-to-peak voltage levels of the oscilloscope without a probe attached. Figure 20 depicts the inherent noise of the oscilloscope.

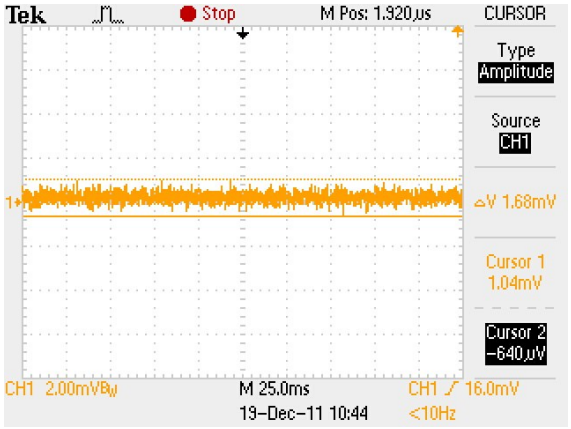

Figure 20. Tektronix TDS 2022B digital oscilloscope screen capture of the inherent noise associated with the operation of the oscilloscope. This was produced by having no probes attached to the oscilloscope.

The next noise floor measurement taken was the oscilloscope with a 1x attenuation probe attached to the input and the probe attached to the output of the Doppler sensor module while the module was not powered. As seen in Figure 21, the

oscilloscope captures 4 mV worth of noise. The last noise floor measured, and the one that will help determine the actual noise floor associated with the Doppler sensor module, is the noise produced by the Doppler sensor module when powered on. This measurement must be taken in a controlled environment, when there is no movement, as to not produce any response by the Doppler sensor module.

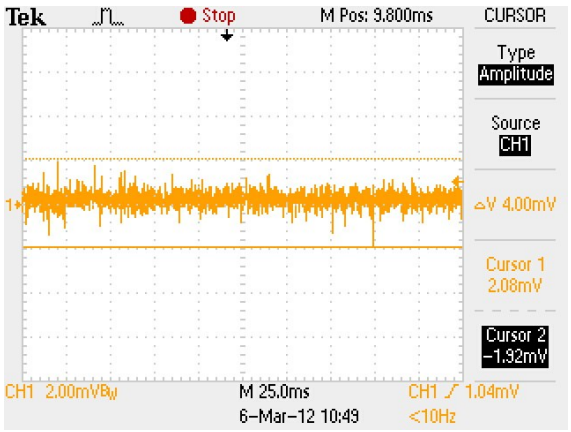

Figure 21. Tektronix TDS 2022B digital oscilloscope screen capture of the inherent noise associated with the operation of the oscilloscope and a 1 × attenuation probe attached to an input on the oscilloscope. The probe was attached to the Doppler sensor module's output and ground with no power supplied to the module.

However, after powering on the Doppler sensor module, no change was observed on the oscilloscope as the Doppler sensor module's noise was buried inside the inherent noise of the oscilloscope and probe. Therefore, in order to obtain a better result, the output of the Doppler sensor was amplified. This amplified noise measurement can be seen in Figure 22. As a result of amplifying the output of the Doppler sensor to obtain its noise floor, the inherent noise of the op-amp and resistors was introduced into the noise floor measurement seen in Figure 22. To combat this issue, a low noise op-amp and reasonable value resistors were used, which should help reduce the effect of the noise

produced by the amplification circuit on the Doppler sensor module's noise. Normalizing the Pk-Pk voltage level of Figure 22 shows a maximum noise level of 220 µV. However, this value is higher than the true noise floor as there is noise from the amplification circuit, the leads of the Doppler sensor module used to connect to the amplification circuit and the inherent noise of the oscilloscope that was documented in Figure 21.

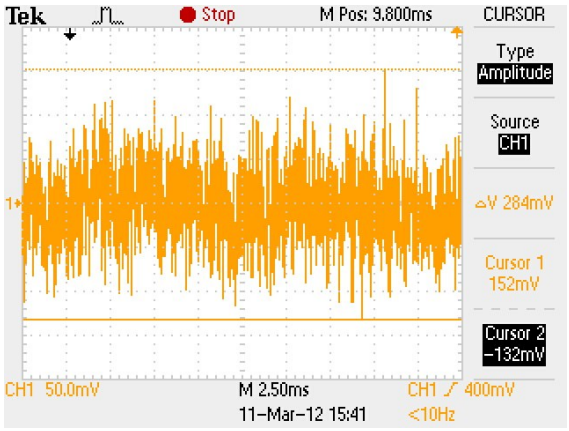

Figure 22. Tektronix TDS 2022B digital oscilloscope screen capture of the noise output by the Doppler sensor module amplified by ~1,250.

Analog Circuitry

With an understanding of the expected output of the Doppler sensor, formalizing what electronic building blocks will be utilized in the analog circuitry block from Figure 4 can begin. The signals will need to be amplified as the expected inputs range from a few µV to a few mV. At a minimum, bandpass filtering will be needed to reduce the noise outside of the expected signal frequencies. Non-linear amplification will also be needed due to the large dynamic range (72 dB) which is proposed to be covered by the microwave rain gauge. After the signals have gone through amplification and filtering, they will need to be digitized in order to interface the circuitry with an embedded

processor. A comparator, used as a Schmitt trigger, can be utilized to create digital logic level signals from 0 V to 5 V for frequency measurements and clipping and limiting circuitry can be used to produce a 0 V minimum and 5 V maximum signal for RSS measurements. A block diagram of the analog signal processing chain can be seen below in Figure 23.

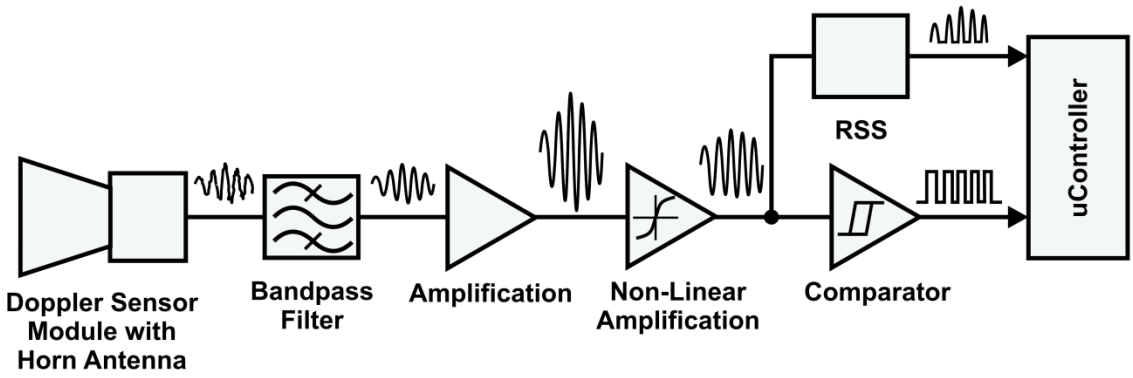

Figure 23. In-depth block diagram of analog signal processing chain from Figure 4. The Doppler sensor is amplified, filtered, non-linearly amplified and digitized before terminating in a microcontroller for further processing.

CHAPTER IV

TESTING METHODOLOGY

In this chapter, the creation and the process of using the test suite is discussed. With the test suite created, a multitude of tests can be run without the need for significant setup, decreasing the amount of time needed for development.

Need for a Test Suite

The ability to test the analog circuitry that will manipulate the output of the Doppler sensor is imperative. Without a testing methodology, the inability to test the extremes of the microwave rain gauge could result in failures which may not be recognized until the device is out in the field. Another source of possible missteps is ensuring that the angle at which the sensor is tilted is 45°, as this is the angle of operation that will be used when placed in the field. While the angle at which the sensor is tilted may only need to be checked once or twice a day to ensure the droplets are consistently being captured under an identical setup, it becomes time consuming. However, if these checks are not performed and it is later discovered that the tilt was off by more than a couple of degrees, the data needs to be manipulated in order to be compared, another very time consuming task.

In addition, it is difficult to reproduce the same size droplet every time to get exact comparisons. Although the differentiation in size of the droplets produced may be inconsequential to the results, the bigger concern, with respect to drop size, is the extreme difficulty associated with producing drops of an extremely small diameter. Another concern is getting the droplets to their terminal velocities. To accomplish this access to a "drop tower" is needed. A "drop tower" provides the ability to produce droplets from a substantial height, making the descent of the artificially produced droplets to more closely mirror the descent of naturally occurring droplets.

Understandably, with respect to all the difficulties listed above, it would be of great benefit to replicate the signal output from Doppler sensor module for many different droplets without the use of the Doppler sensor module. Then, the replicated signals could be fed to the circuitry and be used for testing and validation. Thus, allowing for quicker development time and providing a testing method for the circuitry.

Creation of Test Suite

Producing Droplet Signature

The first thing needed to replace the Doppler sensor module was a signal generator capable of reproducing the droplet signature. Because the droplet signature output by the Doppler sensor is not a common waveform, such as a square or saw tooth waveform, a signal generator was needed that could handle an arbitrary waveform. The Agilent 33250A, pictured in Figure 24, is an arbitrary waveform generator (AWG) that provided such capabilities. An AWG is a piece of electronic test equipment that differs from function generators. AWGs can generate any arbitrarily designed waveform at their output. They normally accomplish this by using a lookup table a user defines that is a combination of specified voltage levels at a specified time. To connect the specified points, AWGs can use many different forms of interpolation; in the case of the Agilent 33250A it interpolates a line. The created waveform can then either be output as a single sequence or repeatedly at a frequency specified by the user.

After determining that this signal generator would be capable of replicating the droplet signature, it became a matter of determining how to generate the signature. The first naïve method of entering each point on the Agilent 33250A by hand was quickly abandoned. This method would not only have been a very long and strenuous process but would have led to poor results. This method was abandoned when the Agilent IntuiLink Waveform Editor software was discovered, which allows communication between the

signal generator and a PC. Using this software, users can create waveforms and load them into the signal generator and output the signal from the signal generator.

Figure 24. Photograph of the Agilent 33250A Arbitrary Waveform Generator.

The Agilent IntuiLink Waveform Editor allows an individual the ability to create any signal imaginable, as there is a freehand tool, in addition to set waves; such as, a square wave, triangle wave, etc. Before loading the desired waveform created by a user onto the signal generator, a few parameters must be set. The two main parameters, relevant to the creation of the droplet signature, are the frequency of the waveform to be output and the peak-to-peak amplitude of the signal. This is necessary due to the fact that specific voltage levels or time intervals are not set when creating a waveform. Rather, everything is done relative to other points inserted onto the screen.

With the use of the Agilent IntuiLink Waveform Editor, a second attempt was made at replicating the Doppler sensor module output using the general knowledge of a typical droplet signature obtained while performing experimental testing for the RSS.

Unfortunately, the use of the freehand tool proved to be inexact and was too much of a variation from the true signature that was observed on the oscilloscope. Another method tried was using some of the set waveforms provided by the software to replicate the signature. This involved using a sinusoidal wave as the base with a varying frequency to represent the droplets moving faster or slower. This was then manipulated by the RSS relationship derived to represent the reduction in RSS due to distance and drop size. Although this method was getting closer to the real signature, it was still messy and cumbersome, requiring hours of calibration and tweaking before realizing a signature that would truly represent the extremes encountered in nature.

As with previous methods, this method was abandoned when the discovery of loading comma-separated variable files into Agilent IntuiLink Waveform Editor produced very good results. This method was exceptionally beneficial as the Tektronix TDS 2022B Digital Oscilloscope, which was being used to demonstrate the inverse power laws, could save a comma-separated value file onto a flash drive. This comma-separated value file not only contained a list of time dependent voltage levels but the setup information on the oscilloscope. While the comma-separated value file included voltage scale, timing scale, probe attenuation setting, etc., this information could not be included when loading the file into Agilent IntuiLink Waveform Editor. In order to maintain the data integrity of the captured waveforms, the relevant data was copied to a new CSV file and saved in order to be loaded onto the Agilent 33250A. Two methods were considered in order to leverage this technology.

The first method involved capturing natural rainfall as it occurred. While this was initially the method that was going to be pursued, it was quickly discovered after a couple of attempts that it would be very difficult to collect data from naturally occurring rainfall without a fully developed device. It became apparent that it was important to shield the electronics from the rain so as to not damage the power supply, oscilloscope or capturing circuitry. While this would not have posed a huge problem had the device been

positioned close to a building, the building's structure blocked a lot of the rainfall and runoff from the roof caused the formation of unnatural droplets. Testing away from a building posed another problem as extension cords were needed to supply power to the regulated DC power supply and oscilloscope. And, lastly, the problem posed by this method was the unknown characteristics of the data being collected. While the data may represent a natural rainfall, the size of the droplets captured would be unknown and, quite possibly, the extreme conditions that the sensor may encounter would not be tested.

After considering the different methods, the method that would allow for the appropriate amount of user control, while capitalizing on time efficiency, was the method that involved capturing a single droplet and leveraging the knowledge gained from the RSS model and of the Doppler frequency equation to manipulate the droplet's signature to match many different droplets.

Table 7. Characteristics of drop captured for use in developing test suite

Diameter of Drop (mm)	3.5
Radar Angle (degrees)	45
Drop Height (cm)	46
Distance from Sensor (cm)	18
Ambient Temperature (C)	22
Gain of Capture Circuit	~1,250

To accomplish this task, the first step was to set up a controlled droplet capture experiment. Parameters that needed to be accounted for included droplet size, angle of the Doppler sensor, height of the droplet from the Doppler sensor, distance away the droplet would pass by the Doppler sensor and the ambient temperature. All of these characteristics can be seen in Table 7.

The output for this setup can be seen in Figure 25. Assuming over the drop distance of ~1 meter, the droplet will not experience effects such as drag and will not reach terminal velocity. Also, because the droplet was created inside a controlled environment with no natural elements, such as wind, the instantaneous velocity of the droplet can be determined, just as if it were a free-falling object. The expression to determine the instantaneous velocity of a free-falling object is stated below

$$v_i = \sqrt{2gd}$$

where $g = 9.8\ \mathrm{m/s^2}$, d is the distance that the object has travelled and v_i is the instantaneous velocity of the object (Halliday et al., 2008).

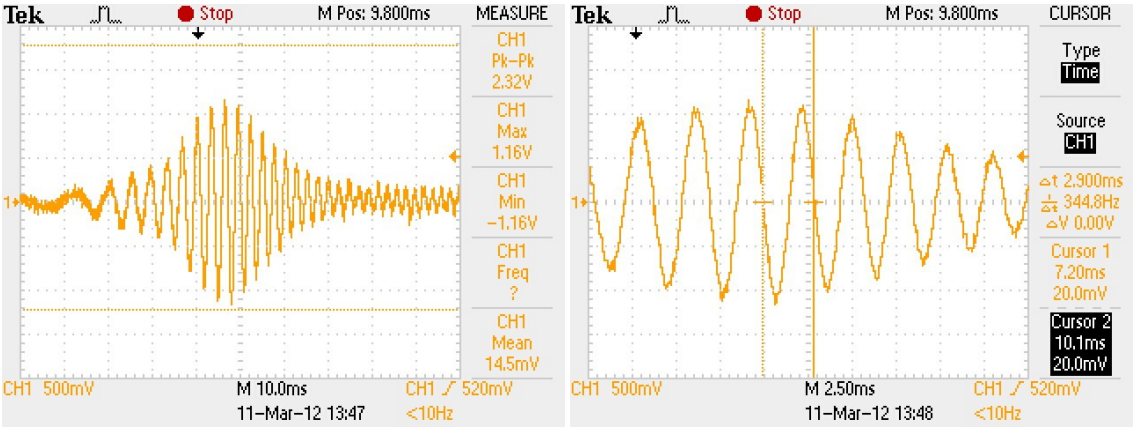

Figure 25. Screen capture of droplet that will be used for test suite.

Using this equation, the velocity of the droplet as it passed the Doppler sensor was calculated. With the assumption that the gravitational force on earth is approximately $9.81\ \mathrm{m/s^2}$, the instantaneous velocity equates to

$$v_i \cong \sqrt{2 \times 9.81\ \frac{\mathrm{m}}{\mathrm{s}^2} \times 0.46\ m} \cong 3\,\frac{\mathrm{m}}{\mathrm{s}}$$

Using the velocity derived from the instantaneous velocity of a free-falling object equation, the screen capture of the oscilloscope was verified by determining the expected Doppler frequency using Doppler frequency equation.

$$f_{\text{Doppler}} \cong 3\ \frac{\text{m}}{\text{s}} \times \cos(45)\frac{2 \times 24.15\ \text{GHz}}{3 \times 10^8\ \frac{\text{m}}{\text{s}}} \cong 342\ \text{Hz}$$

Comparing this calculated Doppler frequency to the one shown in Figure 25 confirms that the values are close enough where variation in exact measurements and assumptions made about the strength of the gravitational field and rounding of the speed of light could account for the differences.

Manipulating RSS for Test Suite

With the capturing and understanding of the droplet signature, many different manipulations to the CSV file will allow it to represent natural rain drops. Because the amplitude of the signal is related to the droplet's size and distance from the device, the amplitudes can be adjusted to match any size and distance. However, a lower limit does exist that causes the Agilent 33250A to interpret the values as zero. This was a cause for concern for almost all the signals that were to be used for the testing of the detection circuitry.

In order to combat this issue, set gains were used that could then be attenuated out by a voltage divider that was directly connected to the signal generator. But, due to the wide range of amplitudes (72 dB) the circuitry was to encounter, one gain was not able to contain all signal levels needed. This is due to the fact, as mentioned earlier, that the smaller a droplet becomes and the further away, the RSS relationship quickly diminishes the signal amplitude. Therefore, if the same gain was used, a large droplet that fell only a couple centimeters from the radar, would begin to get clipped by the signal generator as its maximum output voltage is 10 volts.

The one observation that these RSS manipulations do not take into account is that maintaining the same S/N level for every droplet signature is inaccurate. The noise floor for different droplet sizes should remain ultimately the same. However, by making general amplitude changes the noise level is also increased or decreased along with the signal. To counteract this inaccuracy, the noise floor of the Doppler sensor module that was determined will replace the noise in the RSS manipulated signals. This will allow for a more realistic droplet signature to be loaded into the Agilent 33250A for development and testing.

With the proper measures having been taken to allow for the Agilent 33250A to properly produce the desired signals without any distortion, the method to create the CSV files to load into Agilent IntuiLink Waveform Editor are as follows:

1. Determine the droplet characteristics to be used. For this example, the goal will be to produce a 0.5 mm diameter droplet 6 cm away with a gain of 30.
2. To remove the gain of the captured signal circuitry, divide the Master CSV file's captured signal levels by 1,250.
3. Divide the values determined in step 2 by

$$\frac{\text{Captured droplet diameter in mm}^{1.4}}{\text{Desired diameter in mm}^{1.4}} = \frac{3.5^{1.4}}{0.5^{1.4}} = 15.25$$

4. Divide the values determined in step 3 by

$$\frac{\text{Desired distance in cm}^{1.6}}{\text{Captured droplet distance in cm}^{1.6}} = \frac{6^{1.6}}{18^{1.6}} = 0.17$$

5. Replace manipulated noise with the determined noise floor of Doppler sensor module.
6. Multiply the values determined in step 5 by desired gain, in this case 30.

Using this method, the Doppler sensor module's amplitude for any combination of droplet size and distance can be calculated.

Manipulating Frequency for Test Suite

The other aspect that must be modified to create the signature of a natural rain droplet is the frequency of the signature, which is directly related to the velocity the droplet is falling. As stated earlier, in order to set the frequency output by the Agilent 33250A, a frequency parameter is set when a waveform is loaded onto it from Agilent IntuiLink Waveform Editor. This is important. It is vital to have the relative frequency between different droplets correct, when multiple droplets are strung together.

To modify different droplet size frequencies, a baseline was established using the Maser CSV file. This Master CSV file has 2,500 data points that represent the droplet signature, knowing that as a droplet passed the Doppler sensor module, it produced a frequency of ~345 Hz as can be seen in Figure 25. With this knowledge, a baseline will be set that states 2,500 data points is correlated with a frequency of ~345 Hz. For different fall speeds, more points can be added to lower the frequency or removed to increase the frequency of the signature of other drops to be strung together with the Master CSV signature. A simple ratio of hertz per data points can be used to find the exact number of points needed to create the specific frequencies. Table 8 below shows a few of the calculated number of data points needed to represent specific frequencies in relation to the Master CSV file, as they pertain to specific drop sizes.

Table 8. Number of data points needed in relation to master drop signature

Drop Size (mm)	**Velocity (m/s)**	**Frequency (Hz)**	**# of Data Points**
0.5	2	227	10,518
2	6.5	740	3,226
3.5	8.4	955	2,500
5	9.1	1,035	2,307

Using the Test Suite

With the ability to create a multitude of different droplet signatures and armed with the ability to concatenate droplets so that they follow one another, it is up to the user to pick the sequence which they would like to test, keeping in mind to choose sequences that can be handled by the Agilent 33250A, due to its voltage limits. After determining the desired sequence and ensuring that all values can be handled by the Agilent 33250A, the voltage divider needed to attenuate the signals to their true values must be constructed.

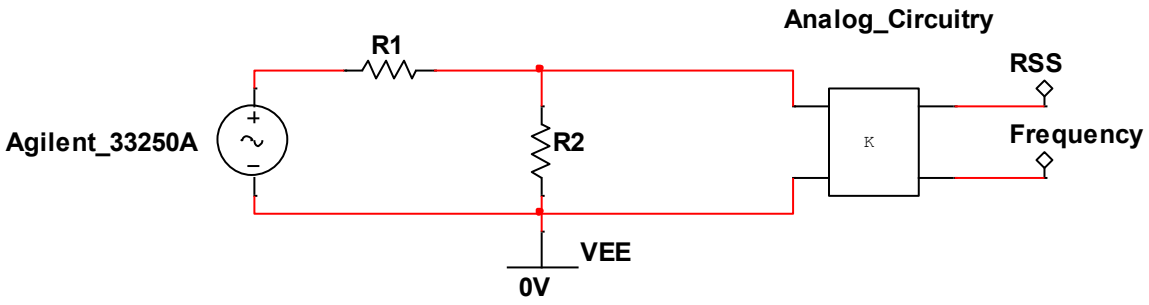

Figure 26. Graphic of the test suite setup. The Agilent 33250A outputs the amplified drop signature and the values are then attenuated by the voltage divider. The voltage divider allows for the signals to be input to the analog circuitry at their true value, as the Agilent 33250A cannot produce values less than 1 mV.

The voltage divider's attenuation must match the final gain applied to the signals. In order to properly attenuate the signals and mimic the signal generator, the attenuator needs an output resistance of 50 ohms. The scheme used is shown in Figure 26 and is controlled by the equations that follow:

$$R_{eq} = \frac{R_2(50 + R_1)}{50 + R_1 + R_2} = 50$$

$$\frac{1}{Gain} = \frac{R_2}{50 + R_1 + R_2}$$

Using a selected gain, along with the calculations from the two equations, the required resistors R_1 and R_2 needed to attenuate these signals to their desired level can be formulated. A few examples have been worked out and shown in Table 9. When constructing the physical circuit, the nearest value resistor should be used. To test the circuitry, the output of the voltage divider should be connected to the input of the analog circuitry.

Table 9. Resistor values used to normalize the output of Agilent 33250A

Gain	**R1**	**R2**
30	1.45 kΩ	51.7 Ω
1000	50 kΩ	50.05 Ω
5000	250 kΩ	50.01 Ω

CHAPTER V

ANALOG CIRCUITRY

In this chapter, the analog signal processing chain is discussed in more detail. More specifically, this includes the process of running the microwave rain gauge sensor off of a battery. The hardware for a microwave rain gauge sensor, including an in-depth look at the non-linear amplification strategies, is explored. Finally, the measures taken to properly digitize the analog signal to digital logic levels for use by an embedded processor are discussed.

Power Supply

A key requirement of the device is that it be battery operable for remote deployment. Since batteries are not regulated and do not provide short circuit protection, the first task is to create a short circuit, reverse polarity protected, well regulated power supply for use throughout the microwave rain gauge. Because noise is a large concern, linear regulators will be used instead of switching regulators to regulate the voltage to the needed levels. To provide reverse bias protection, a Schottky diode will be placed in line with the unregulated positive terminal of the battery. This ensures that the current flows in only one direction. To provide short circuit protection, a fuse is inserted in series with the diode. The components chosen for the final design require 10 V, 5 V and 3.3 V for operation. The schematic for the power supply circuitry is in Figure 27.

Also, since batteries supply only two reference points, a third reference point will need to be derived to accommodate components such as op-amps that require a positive, negative and, for many applications, a ground, to bias the op-amp. Two possible solutions were considered for use in the microwave rain gauge sensor. The first option was creating a negative voltage. The second option was creating a virtual ground. While both options produce the same result having created a positive, negative and ground

reference, they require different steps to build and there are tradeoffs to consider. Both options have ICs that are readily available and will complete the desired task.

To create a negative voltage, the TC962, a high current charge pump DC-to-DC converter, can be used. The TC962 uses switched capacitors to produce a negative voltage. However, care must be taken in regards to the current needs of components to which it will supply, as it can only supply 80 mA. Methods do exist to increase the current capabilities, such as putting multiple TC962s in parallel to provide a larger current reservoir. However, in the application of the microwave rain gauge sensor, component count will be fairly low and current consumption needed should be well within the confines of 80 mA for the analog circuitry portion. A major drawback of the TC962 is that the switch capacitors can lead to noise on the power supply rails.

Creating a virtual ground is accomplished by halving the positive rail in reference to true ground. Once this virtual ground has been created, the true ground can then be thought of as the negative rail. A simple workable solution is to use two equal value resistors to create a voltage divider. Although this works, resistors change with temperature and to truly produce half of the voltage, components would need to be analyzed to match due to tolerances leading to slightly different characteristics. An alternate solution is using a rail splitter, such as the TLE2426. The TLE2426 outputs precision virtual ground whose output voltage is always equal to one-half the input voltage. The output of the TLE2426 will now be thought of as ground for the rest of the circuit. A minor downside to using a rail splitter is that the voltage range for a 10 V input voltage is still 0 to 10 V. Unlike, when using the DC charge pump to create a negative voltage the range would be -10 to 10 V. The voltage range is not a major issue but must be considered due to outputs on most op-amps not being able to go above or below their supply rails. For these reasons, the TLE2426 was chosen in order to produce the needed reference voltage.

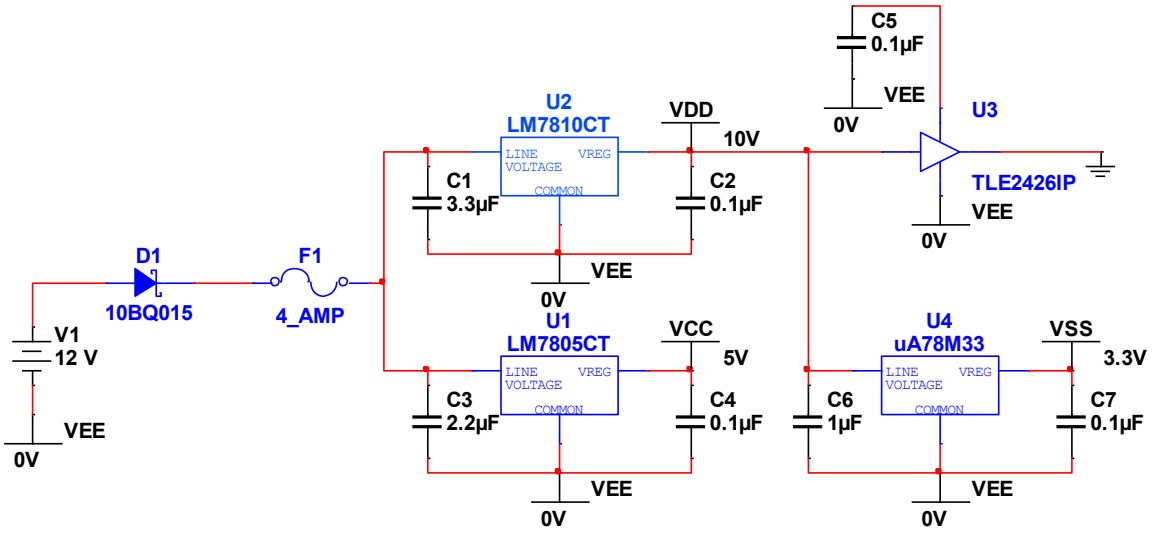

Figure 27. Schematic of the power supply circuitry used to provide power to ICs as well as creating a virtual ground to refrence the ICs.

Bandpass Filter

One way to increase the S/N ratio is by reducing the noise in the system. An effective way to reduce noise is to reduce the bandwidth of the signal. As discussed earlier, this is due to the fact that noise is directly related to the bandwidth of the signal. The passband of the filter are clearly defined by the expected minimum and maximum frequencies described in Table 3.

A bandpass filter, with cutoff frequencies set at the minimum and maximum expected frequencies, will provide the best benefit for filtering unwanted frequencies. There are many different ways to produce bandpass filters. Whether or not to use an active filter or a passive filer is the first decision which needs to be made. Two of the major downsides to an active filter are that power is required and they have limited bandwidth; however these are moot points in this discussion as power is already necessary for the microwave rain gauge and the frequencies are well within specification of a large majority of op-amps. Other drawbacks of active filters include noise which may be interjected from the op-amps chosen for implementation. This noise can be

limited by choosing low noise op-amps such as the OPA2228. Two advantages of active filters are that gain can be set in the passband and the output impedance of the filter is very low. The low output impedance will make the design of other blocks easier as loading effect will not alter the active filters characteristics.

Passive filters, on the other hand, do not require power and are constructed of passive components such as resistors, capacitors and inductors. For this reason, passive filters are less noisy and the noise that is produced is inherent to the components chosen. However, because of the passive nature of the filter, there is insertion loss that will occur in the passband, causing some slight degradation of the theoretical benefits of a passive filter.

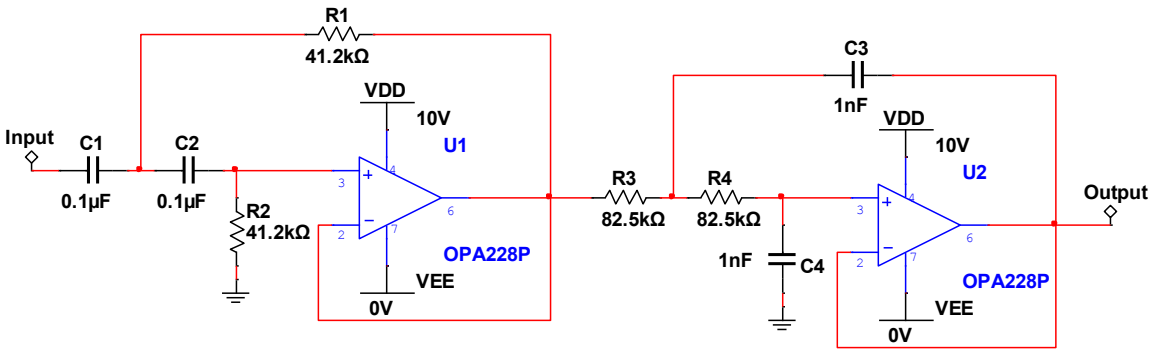

Figure 28. Hardware schematic for the 4th order bandpass filter with cutoff frequencies of 61 Hz and 1.25 kHz. The filter consists of a high pass 2nd order Butterworth filter and a low pass 2nd order Butterworth filter.

With the ability to add gain if desired and the attractiveness of low output impedances, active filters will be used. In an effort to keep as little ripple in the passband as possible and to keep gain fairly constant throughout the passband, the bandpass filter will be constructed of a second order, equal component, unity gain, high pass Butterworth filter and a second order, equal component, unity gain, low pass Butterworth filter. The

bandpass filter schematic can be seen in Figure 28. Although in theory the order in which the filters are placed does not matter, for the microwave rain gauge, it will be beneficial to place the high pass filter first in order to properly bias the output of the Doppler sensor as it has a small DC offset voltage.

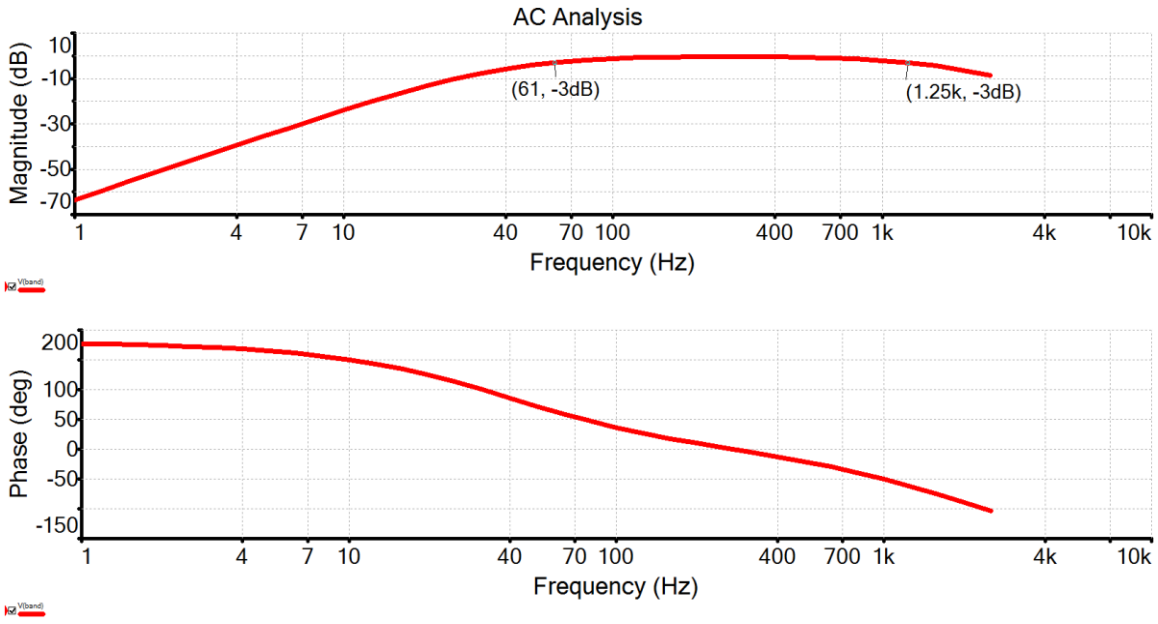

Figure 29. Bode plot of the bandpass filter seen in Figure 28.

The cutoff frequencies chosen from Table 3 are used to choose the components. The equation used to determine the cutoff frequencies is

$$f_o = \frac{1}{2\pi RC}$$

where f_o is the cutoff frequency for the filter, R is the resistor value and C is the capacitor value. Since the cutoff frequency desired is known, an arbitrary value must be selected for R or C in order to solve for the other. It is usually best to select C first, as there are less standard values for capacitors than there are for resistors. To obtain the best results, the use of low tolerance components is also beneficial to more closely match the

theoretical calculations. However, since this formula is for idealized op-amps, their actual results may differ when implemented. A better design solution is to simulate the bandpass filter using SPICE and adjusting values accordingly. The simulated amplitude and phase response of the bandpass filter can be seen in Figure 29. As expected, the passband has almost no gain and the -3 dB points are located at the required cutoff frequencies.

Amplification

With the voltage levels output by the Doppler sensor ranging from a few µV to a few mV, it would be beneficial to amplify these signals to a more manageable level. In order to amplify the signals, a simple non-inverting amplifier was constructed (Neamen, 2007). The gain of the non-inverting amplifier needed to be such that clipping of the largest signal was not possible. Looking at Table 6, the maximum expected peak-to-peak voltage is 46 mV. Since the op-amp will be run off 10 V and 0 V and, from experimentation it was determined it can output near rail to rail, the maximum gain should be set to as high as possible without clipping.

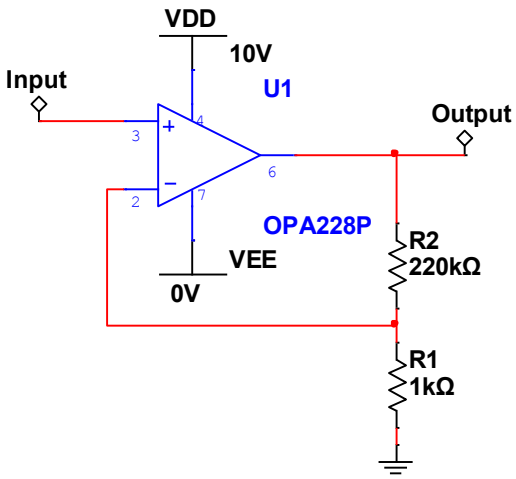

Figure 30. Hardware schematic for non-inverting amplifier with gain of 221.

The maximum gain possible in the initial amplification stage can be determined by dividing 10 V by 46 mV. The result is

$$Max\ Gain = \frac{10\ \text{V}}{0.046\ \text{V}} = 218$$

Accounting for the fact that a small majority of droplets will fall that will produce the max signal from the Doppler sensor module, the final gain was set at 221. The schematic for the non-inverting amplifier used in the analog signal processing chain can be seen in Figure 30. An updated magnitude plot is also shown in Figure 31.

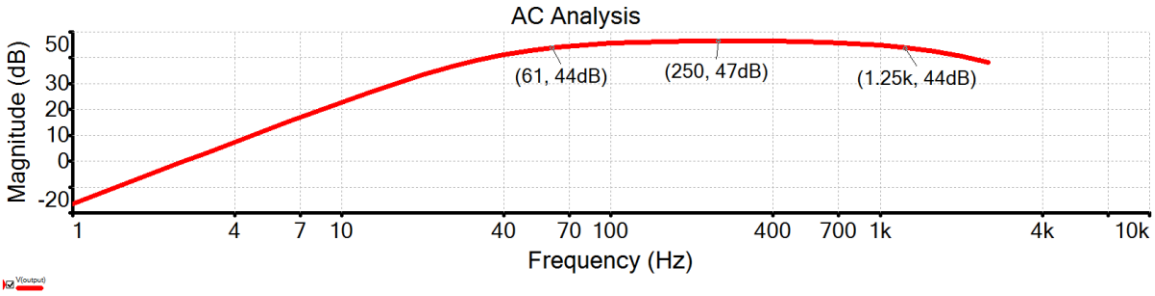

Figure 31. Plot of the magnitude response after being filtered and amplified. Note that a gain of 221 is approximately 47 dB.

60 Hz Notch Filter

As mentioned earlier, filtering of 60 Hz noise is of great concern due to the susceptibly of the Doppler sensor modules to AC mains pickup. Since the minimum expected frequency is close to 60 Hz, a low pass filter does a poor job of attenuating the 60 Hz noise. A viable solution to attenuate specific frequencies is a notch filter. Two possible solutions for attenuating 60 Hz noise were investigated.

In a desire to attenuate 60 Hz noise, a very suitable integrated circuit is the LMF90CCN. The LMF90CCN is a 4^{th}-order elliptical notch filter that can be easily

configured to remove 60 Hz noise. The only external component needed is a 3.579545 MHz oscillator, which controls the center frequency of the notch bandwidth. This filter provides 39 or 48 dB of attenuation around the selected center frequency, in this case 60 Hz, and the notch bandwidth is a set percentage of the center frequency selected. However, the LMF90CCN is no longer in production.

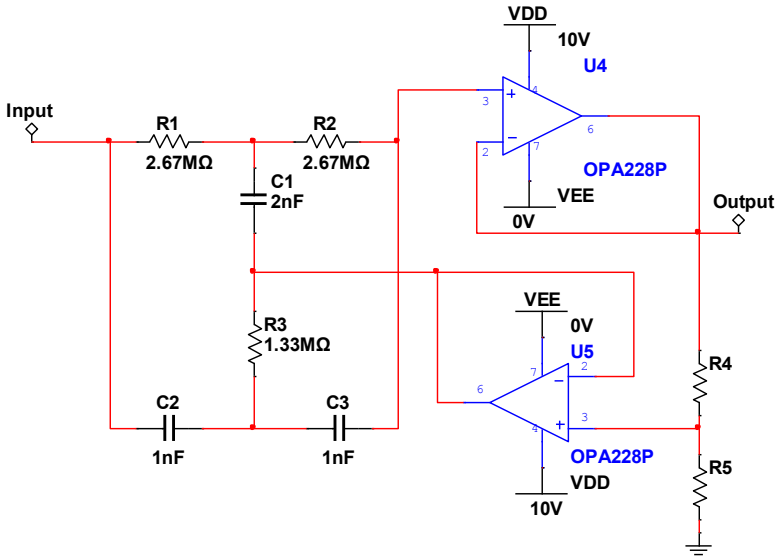

Figure 32. Hardware schematic for twin-t notch filter with notch frequency ~60 Hz.

Another viable solution is the use of a twin-t notch filter. The twin-t notch filter works by phase shifting the signals in the two legs of the filter and then adding the signals at the output. At the desired notch frequency, the signals are 180° out of phase. Consequently, when summed together, they create a null in the signal at the notch frequency. The effectiveness of the notch filter is highly dependent upon matching, as close as possible, the resistors and capacitors. For this reason, 1% resistors and capacitors were used and then component matching was performed by measuring the values of the actual components. The closer the values are matched, the greater the

attenuation will be at the notch frequency. Although the twin-t notch can be created using only passive components, the addition of a couple of op-amps gives greater flexibility and tuning of the notch filter (National Semiconductor Corporation, 1969). The schematic of the twin-t notch filter used in the design of the microwave rain gauge can be seen in Figure 32.

The first op-amp is used in a voltage follower setup, allowing for low output impedance from the notch filter stage, which reduces loading effects on the notch filter. The second op-amp is used to control the *Q* of the twin-t notch filter. The *Q* also plays a role in determining the depth of the notch and the bandwidth of the notch. The *Q* of the twin-t notch filter can be manipulated by adjusting the resistor ratio at the positive input of the second op-amp. A magnitude and phase plot for the output of the twin-t notch filter is shown below in Figure 33.

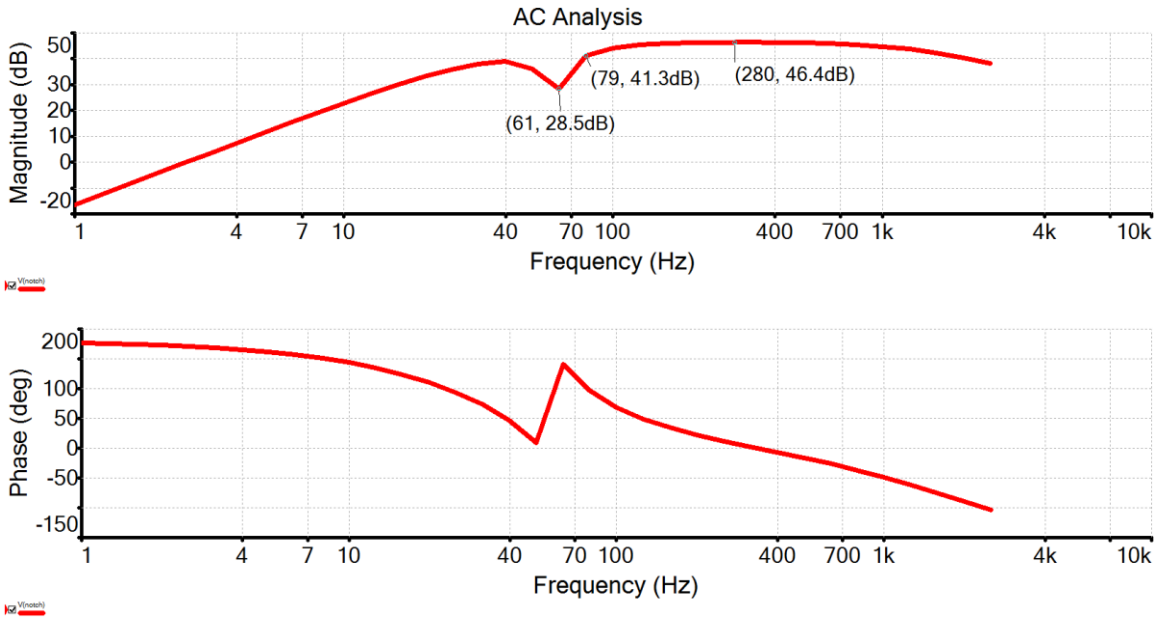

Figure 33. Bode plot of the signal after passing through the bandpass filter, amplification and twin-t notch filter with notch frequency of ~60 Hz.

Non-Linear Amplification

Due to the large dynamic range of the signals (72 dB), linear amplification would result in distortion of large signals from too much amplification or loss of small signals from not enough amplification. Thus, some sort of dynamic range compression is required.

A number of automatic gain control (AGC) schemes, including logarithmic amplifiers were investigated. AGC does not apply, since these schemes are designed to adjust the gain as the signal level slowly fluctuates, and the time constants are typically 500 ms or more. However, the signal levels for the microwave rain gauge fluctuate from droplet to droplet, and the time scale is a few hundred microseconds. Simply changing the time constants of AGC designs does not work and can lead to instability or simply setting the amplifier gain to some average value.

An investigation of logarithmic amplifier ICs was also conducted but many of these devices produce a logarithmic envelope of the signal instead of the instantaneous log of the signal, in which case, the frequency of the signal would be lost. Still other logarithmic amplifiers did not meet the temperature requirements required for the microwave rain gauge. As a result of not being able to find a suitable IC to fit the needs of the microwave rain gauge, a simple but effective method was implemented to perform non-linear amplification to compress the dynamic range of the signal.

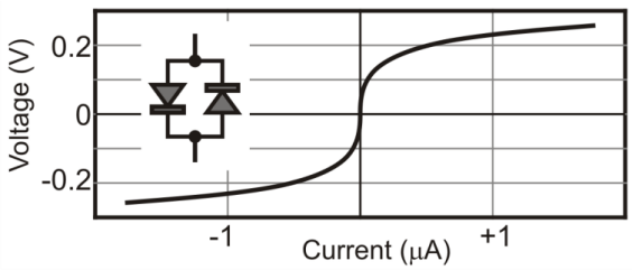

Figure 34. Schematic of a non-linear gain stage and its voltage to current characteristics.

Figure 35 shows the schematic of this simple solution that takes advantage of the logarithmic-like properties of diodes to produce a non-linear gain stage. In Figure 34, it can be seen that two diodes connected as shown exhibit the following non-linear relationship (Malik, 1995)

$$I = 2I_s \sinh(V/V_t)$$

Here, I and V are the current through and voltage across the pair respectively, I_s is the reverse leakage current and V_T is the thermal voltage of the diodes. This can be used to construct a non-linear resistor and incorporate that into a voltage divider, as done in Figure 35.

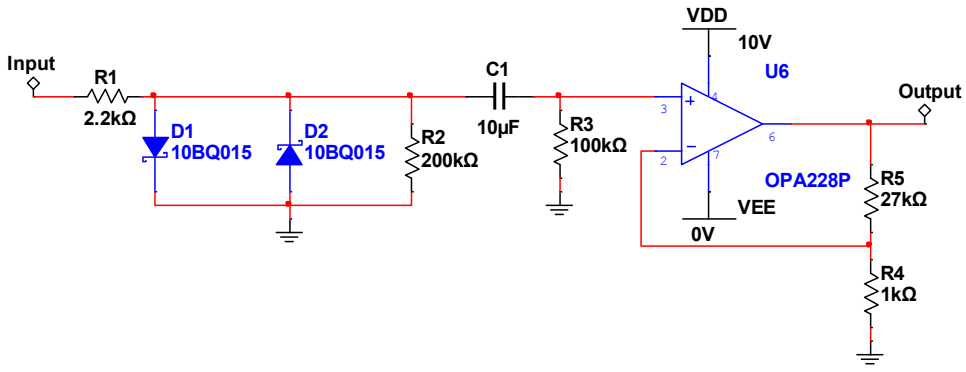

Figure 35. Hardware schematic for non-linear amplification stage. Voltage levels greater than the forward voltage of the Schottky diode are compressed by the back to back diode configuration, while voltage levels less than the forward voltage experience near unity gain. After the compression the signal is re-biased at 5 V to account for offset voltages introduced by the previous op-amps and then amplified 28 times.

Properly designed, such a voltage divider will attenuate large signals, but small signals will pass unattenuated. The circuit shown will limit the maximum voltage to approximately the forward voltage of the diodes and is then amplified by the non-inverting gain stage. The amount of compression can be changed by selecting different

diodes (i.e. Schottky, silicon, etc.) or by adding diodes in series to create larger forward voltages. However, due to the fact that this equation assumes matched diodes, it would be wise to use a diode array IC. Such diodes are on the same substrate, with closely-matched characteristics, leading to a closer equivalent to the theoretical result. The output of the non-linear gain stage for different input voltages can be seen in Figure 36.

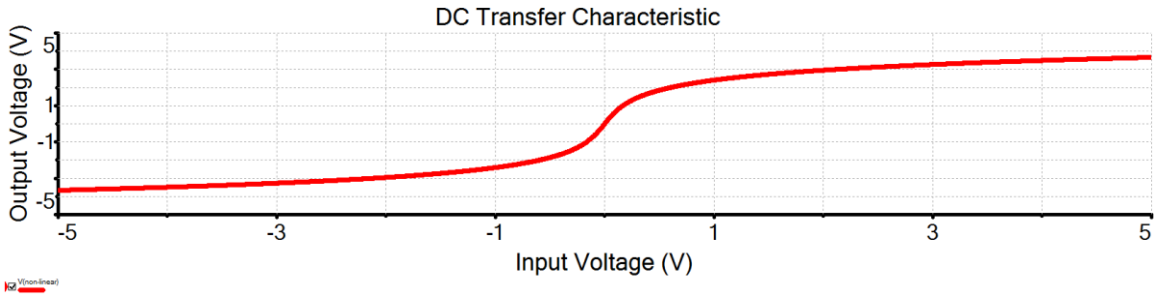

Figure 36. Plot of input voltage versus output voltage of the non-linear amplification stage as seen in Figure 35.

Digitization

With the analog processing chain manipulating the signal to more workable signal levels, the final step is to digitize the signals so that an embedded processor can process the RSS and Doppler frequency.

RSS

To recover the RSS, an analog to digital converter (ADC) can be used. Since most ADC can accept input voltages of 5 V maximums, the peak value input to the ADC must be limited to 5 V. Also, because the microwave rain gauge should be able to record the voltage of each peak of the droplet signature to determine the RSS, averaging will not be considered. To maximize the resolution in which the ADC can measure, it would be advantageous to only pass the positive portion of the signal limited to 5 V. Another

consideration which needs to be made is that throughout the system, the use of a virtual ground has been used, with 5 V acting as virtual ground for the circuit. To make the RSS more universally measurable, it would be advantageous to level shift the signal by -5 V.

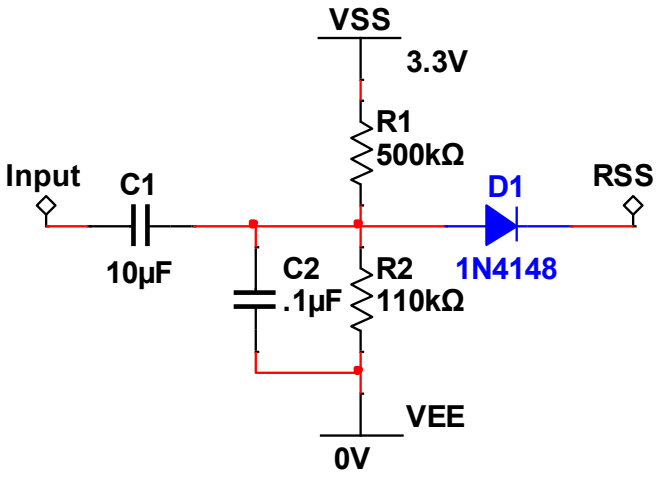

Figure 37. Hardware schematic for level shifting and limiting the RSS to positive signals with an upper limit of slightly less than 5 V.

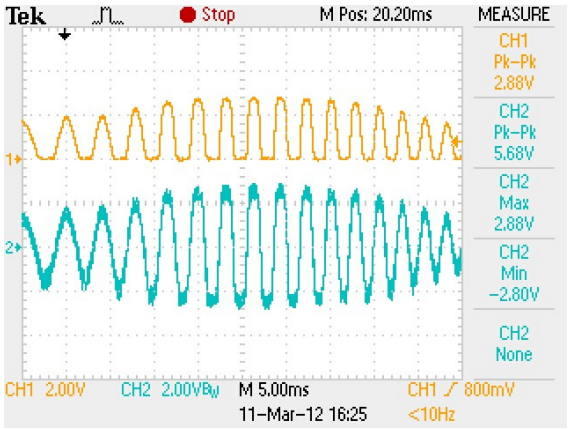

Figure 38. Channel 1 is the RSS output of the analog circuitry that will be fed to the ADC of the embedded processor. Channel 2 is the input that was fed into the RSS circuitry for manipulation.

A simple circuit that can accomplish all of these requirements is shown in Figure 37. The coupling capacitor is used to block the DC offset used by the rest of the system. Through the use of a voltage divider, a new DC offset can be created, which is necessary to compensate for the voltage drop of the diode which will be used to block the negative portion of the RSS. Ideally, it would be nice to match the DC offset created by the voltage divider to the exact forward voltage of the diode. Since this may be hard to accomplish and components are variant over temperature, it is best to include a small buffer in the DC offset voltage of approximately -100 mV as compared to the forward voltage of the diode to ensure the voltage is limited to less than 5 V. The output of RSS circuitry can be seen in Figure 38.

Frequency

To digitize the frequency, a Schmitt trigger can be used. The hysteresis of a Schmitt trigger is set externally by the resistor values chosen. The amount of hysteresis needed is set by the peak values of the noise at the input of the Schmitt trigger. Since a digital oscilloscope is limited in the amount of information it can supply in regards to noise figures, the hysteresis levels set for the Schmitt trigger were done via a guess and check method. A typical value was chosen from observation of the oscilloscope and was continually increased until no false positives were produced while everything was powered on and the Doppler sensor was providing an idle input signal. The final amount of hysteresis incorporated into the Schmitt trigger was 50 mV.

A comparator is well suited to produce a Schmitt trigger. Since the collector of the output BJT on most comparators is left floating, it provides an opportunity to set the high value of the output. Connecting the BJT's emitter to a pull-up resistor connected to the output of the 5 V linear regulator, the high value of the Schmitt trigger is set to 5 V. The low value is selected by connecting the emitter of the output BJT to the desired reference. In the case of the microwave rain gauge sensor it is desirable to set this to 0 V.

The Schmitt trigger will now produce a common digital logic level square wave with output ranging from 0 to 5 V and the frequency will be directly related to the Doppler frequency. A schematic of the Schmitt trigger can be seen below in Figure 39. The output of the Schmitt trigger in comparison to the drop signal can be seen in Figure 40.

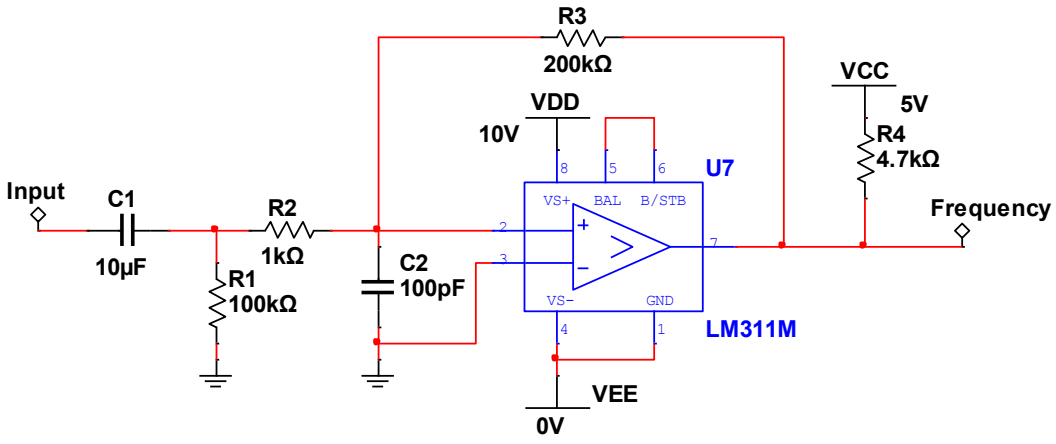

Figure 39. Hardware schematic for transforming the droplet signature into a square wave with a high voltage of 5 and a low voltage of 0.

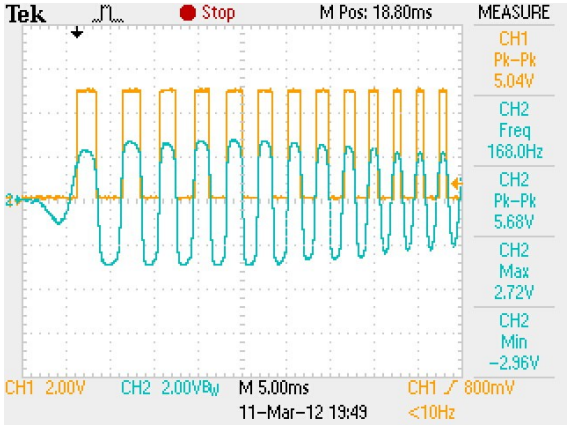

Figure 40. Channel 1 is the frequency output of the analog circuitry that will be fed to the embedded processor for frequency calculation. Channel 2 is the input that was fed into the comparator for manipulation.

CHAPTER VI

EMBEDDED PROCESSOR

In this chapter, the selection of a microprocessor and the process used to interpret the data provided by the analog circuitry is discussed, as well as, interfacing a temperature sensor and an angle of operation sensor with an embedded processor. Using an embedded processor will provide a serial interface, allowing data to be collected easily without additional interface electronics.

Microprocessors

A microprocessor can be used to interpret the output signal of the Schmitt trigger and transform the information into something interpretable to humans. When selecting a microprocessor, a few features that must be considered are analog to digital converters (ADCs), serial communication, external interrupts and timers. In order to give more precise received signal strength readings, it would be advantageous to have large bit ADCs; however, as the number of bits continually increases, the guaranteed accuracy begins to decrease. The accuracy can be increased on some ADCs by calibrating the units or carefully selecting any external components. Serial communication is necessary in order to provide the means to communicate between the device and a computer or data logger. External interrupts are of importance as this will allow the microprocessor to more precisely measure the frequency of the signal output by the Schmitt trigger, versus a less precise polling method. The inclusion of a counter will provide an easy way to keep track of the width of the pulse output by the Schmitt trigger, as well as, be used to determine when an ADC reading of the received signal strength should be taken. Two examples of devices that meet all of these requirements are the Rabbit LP3500 (FOX) and the ATmega128.

Rabbit LP3500 (FOX)

The Fox is a single board computer that contains all of the features needed to interpret the signals output by the microwave rain gauge. A desirable feature of the Fox is that no setup is required to interface the Fox with many peripherals. The Fox comes equipped with pull up resistors, protection circuitry, etc. - all of which are contained on a board about the size of a credit card, as can be seen in Figure 41 (Digi International Inc., 2008).

The Fox uses Dynamic C for developing code and programming the device. Anyone with a background in C programming should not have problems programming the Fox as Dynamic C is closely related to C. The major difference between Dynamic C and C is that Dynamic C comes with built-in functionality for use in embedded systems. For example, multitasking is accomplished through the use of costatements and cofunctions.

However, upon unpacking the device, the downside to the Fox becomes evident as it is essentially completely setup. Some of the general purpose input output pins, GPIOs, are not accessible as they have been used for separate applications. An example of this is the ADCs. On the Fox, the ADCs have been interfaced through a dedicated IC and require communication between the IC and the microprocessor. For this reason, the analog-to-digital conversion using the Fox necessitates more instruction cycles to complete than would have been required had the ADCs been built directly into the microprocessor. Since high accuracy timing is imperative to a good overall system, this is undesirable. A benefit of the dedicated IC is that the ADCs can handle voltage levels up to 20 V. In most cases, ADCs cannot handle voltage levels greater than the reference voltage but the Fox buffers the ADCs' input and allows for larger voltages to be input. Another characteristic not found inherent to the Fox is a rollover interrupt for counters. As stated before, this would be beneficial for more accurate timing.

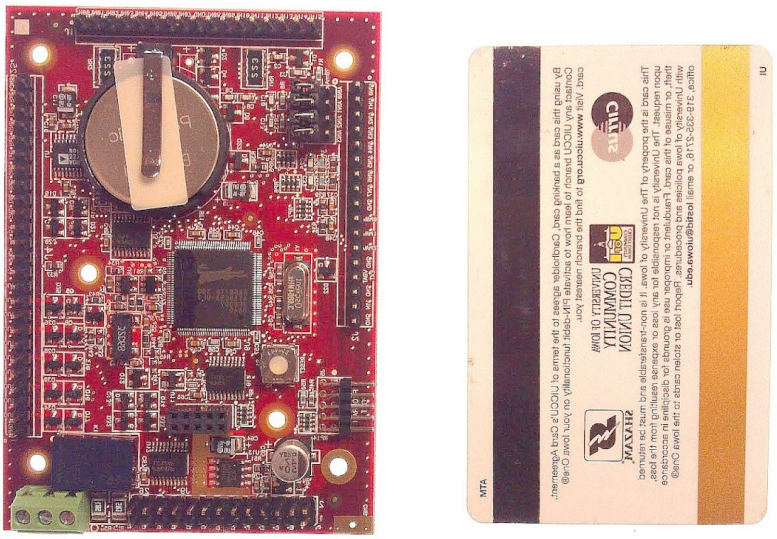

Figure 41. Photo of Rabbit LP3500 (FOX) single board computer. The microprocessor is located in the center of the printed circuit board. The surrounding components allow for fast start up by requiring little to no modifications for processes such as powering on the microprocessor, serial communication and so on.

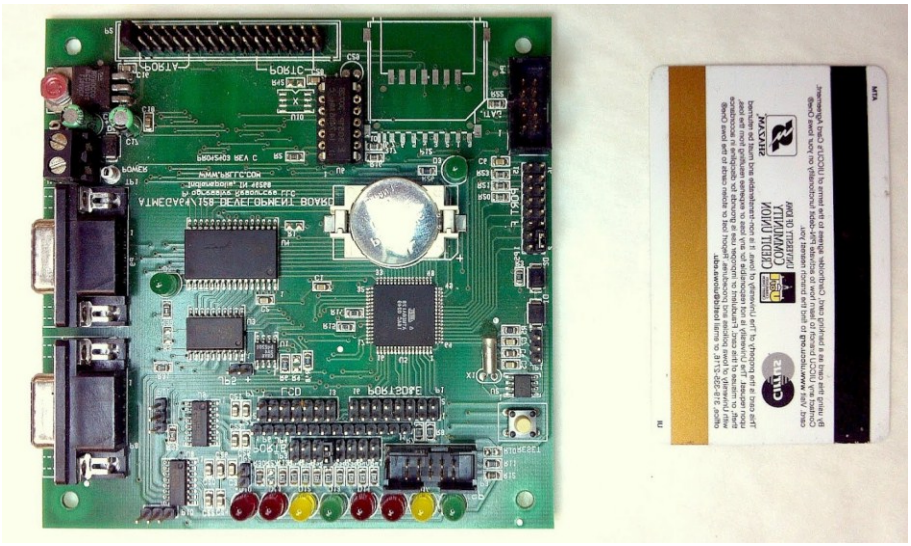

Figure 42. Photo of Mega128DEVelopment Board. The microprocessor is located in the center of the printed circuit board. The surrounding components allow for fast start up by requiring little to no modifications for processes such as powering on the microprocessor, serial communication and so on.

ATmega128

The ATmega128 is a microcontroller that includes all of the features necessary to interpret the signals output by the microwave rain gauge. However, unlike the Fox, the ATmeag128 does not normally come on a development board. Third party manufacturers have created development boards which can be purchased for an additional cost and provide many of the same time-saving features as the Fox.

The ATmega128 does provide a rollover interrupt for timers which will allow for easier timing measurements. Two 16-bit counters is yet another beneficial feature of the ATmega128. The largest counter on the Fox is 10-bit. Since the ADCs are built directly into the ATmega128, this will cut down on conversion time.

Unlike the Fox, the ATmega128 does not buffer inputs and voltage thresholds must be considered when interfacing with devices in order to ensure proper operation of the ATmega128. GPIOs on the ATmega128 cannot exceed the supply voltage plus half a volt and cannot drop below negative half a volt (Atmel Coporation, 2011). Depending on the reference voltage selected to use with the ADC, the maximum and minimum value detectable by the ADC will differ. However, the input voltage allowable on the ADC input pin ranges from ground to the supply voltage. If one uses a reference voltage lower than the supply voltage, then anything over this reference voltage will be output as a maximum value by the ADC. While these voltage constraints were considered when designing the outputs of the microwave rain gauge and are maintained to be within specification, they will need to be considered when choosing peripherals.

Since high accuracy timing is imperative to a good overall system, the advantages provided by the ATmega128 make it an excellent choice. To ensure proper setup and to shorten the amount of time needed for development, an ATmega128 development board was used which provided all the functionality needed. The development board used was the Mega128DEVelopment Board by Progressive Resources LLC and can be seen in Figure 42.

Pseudo Code

```
Set External Interrupt to Fire on Rising Edge
External Interrupt Service Routine{
If Timer is not Running
      Start Timer and Enable Rollover Interrupt
Else
      Calculate Frequency (Method Below)
}
Rollover Interrupt Service Routine{
Increase Rollover Counter++
}
Calculate Frequency{
Pulse Width = Read Timer
If Valid Time Add Pulse Width to the Moving Average Pulse Width
Calculate Time to Measure RSS by using 1/5 of Pulse Width
Turn on Timer Comparator Interrupt set to RSS Measure Time
Reset Rollover Counter and Timer
}
Timer Comparator Interrupt{
Sample ADC multiple times and store the peak value as the RSS value
If Valid ADC Add Voltage to Moving Average RSS Voltage
}
Main{
Initialize Board
Every # Seconds{
Read Temperature IC
Read Accelerometer IC
Output Average Frequency, Average RSS Voltage, Temperature and
Accelerometer Readings over RS-232
Reset Average Values and Counters
}
```

Figure 43. The pseudo code above can be employed to ensure proper operation of the ATmega128 to properly interpret the outputs of the microwave rain gauge sensor. Although some ideas are specific to the ATmega128, such as counter rollover interrupts, many other microcontrollers provide similar functionality.

Calculating Frequency

With the highest frequency expected to be around 1250 Hz, this calculates to a period of 800 µs. At 1249 Hz, 800.64 µs. In order for the calculation to be within an accuracy of a Hertz, the counter used must be able to measure in increments of at least 640 ns. The ATmega128 consists of several counters which provide accurate timing making it ideal for calculating the frequency of signals. The precision of these timers is controlled by the frequency in which they are clocked. The ATmega128 development board runs the microcontroller at 14.7456 MHz using an external oscillator which translates to a 67.8 ns clock cycle. Since the timer can be run off this clock directly, with no pre-scaling, the precision of 1 Hz can be met. However, the lowest frequency expected is around 60 Hz which translates to 16.7 ms, which when divided by 67.8 ns, equals 245,821 clock cycles. The largest counter provided by the ATmega128 is 16-bits and therefore can only accommodate a count up to 65,535. In order to combat this limitation, the ATmega128's rollover interrupt can be utilized when the counter rolls over from 65,535 to 0. Using this interrupt, a variable can be incremented each time the interrupt fires. By using a variable, a third 8-bit register is essentially being added to the counter making the timer precise to the Hertz and operable over the entire expected frequency range.

With the timing capabilities of the ATmega128 able to handle the specifications for the rain gauge sensor, the interfacing of the analog circuitry to the digital circuitry is straightforward. A naïve approach to controlling the timer is to continually poll the input to see when its input value has changed. However, a better approach is using an external interrupt which will implement the process of polling the input in hardware. Setting the interrupt to fire on a rising edge will ensure the square wave output of the analog circuitry will trigger the interrupt. If the timer is not running when the interrupt fires, then the timer should start. If the timer is running, the interrupt should read the timer registers and the overflow counter value. With these values read, the number of clock cycles that have

passed since the last external interrupt fired can be calculated by using the equation below

$$Clock\ Cycles = 65536 \times overflow + 256 \times high\ register + low\ register$$

Once read, the counters should be reset and the overflow variable set up for the next frequency reading. The values calculated during the interrupts will be added to a moving average. The moving average value of the clock cycles can be converted to average frequency by dividing the main oscillator frequency by the average clock cycles.

RSS

To determine the RSS, the fact that the peak value happens at one-fourth the period of the drop signature should be used. The timers in the ATmega128 also incorporate a match register. When the timer matches the value in the register, an interrupt is triggered. During the external interrupt for calculating the clock cycles, the match register should be set to one-fourth the value of the clock cycles, which is in fact one-fourth the period. During the match register interrupt, an ADC reading can be made of the RSS.

Although this approach is sound in theory, it does not take into account the fact that ADC readings are not instantaneous. The ATmega128 datasheet states that a normal conversion takes 13 ADC clock cycles. The first conversion after the ADC is switched on takes 25 ADC clock cycles in order to initialize the analog circuitry (Atmel Coporation, 2011). To eliminate the problem posed by the first conversion having different timing requirements, an ADC measurement can be made at program start up. The ADC clock is a scaled value of the main oscillator of 14.7456 MHz, for this application the ADC clock will run at 921,600 Hz. This means that a normal ADC reading will take 14.1 µS. However, the ADC in the ATmega128 uses a sample and hold feature that will hold the analog voltage value after 1.5 ADC clock cycles after the start of a conversion. This means the voltage read by the ADC is actually the value 1.6 µS

after the start of the conversion process. By using the above method at high frequencies, the peak RSS value could be missed.

A better approach, which would allow for some timing leniency, is to make multiple measurements starting slightly before the one fourth pulse width stated above and only choose the maximum value and return this as the peak RSS value. By sampling the input the peak RSS value will be captured on a more consistent basis. These peak RSS values will also be gathered in a moving average value.

To transform the analog to digital conversion to a meaningful output, the digitally stored average peak RSS value must be converted back to its analog voltage. Since the ADCs on the ATmega128 are 10-bit, the increments that the values are measured in are 1/1024 of the reference voltage. In the case of the microwave rain gauge, a reference voltage of 5 V is used. Therefore, the ADC can measure in increments of 4.88 mV. To convert the digitally stored value, simply multiply the value by 4.88 mV to arrive at the analog average peak RSS value.

Angle of Operation

To determine the angle of operation, an accelerometer was employed. An accelerometer measures the gravitational force acting on the IC in the X-axis, Y-axis and Z-axis. The IC chosen for this particular application was the ADXL335. An image of the accelerometer on a breakout board is seen in Figure 44.

This accelerometer outputs its data as analog voltages for each axis that can be read using the ATmega128's ADCs (Analog Devices, Inc, 2009). The voltage output by the accelerometer is also ratiometric, meaning that the output will differ with the supply voltage applied to the IC. For instance, 0 g is set to half the supply voltage. So, if the supply voltage is 3 V, the output is 1.5 V but if the supply voltage is 3.3 V, the output for 0 g is 1.65 V. Using a 3.3 V regulator to power the ADXL335 sets the bias voltage at 1.65 V and each g changes the analog voltage by ±330 mV, typical. The ADXL335 is

capable of measuring up to ± 3 g; however, because the gravitational effect being measured is static, the highest possible g's experienced by the sensor is ± 1 g. Outputting the raw data from the ADXL335 will allow for the end user to determine the angle of operation of the rain gauge. If the user wishes to operate the device at a 45° angle, it would require that two of the axes outputs be equal, the specific axes depends on the orientation of the IC.

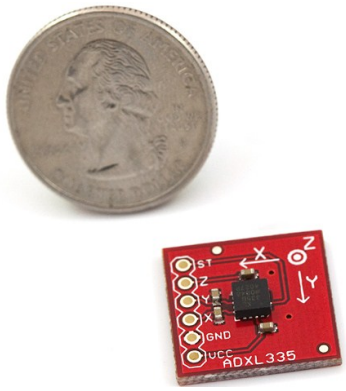

Figure 44. Photograph of the ADXL335 mounted on a breakout board. The accelerometer is used to determine the angle of operation of the microwave rain gauge.

Ambient Temperature

To determine the ambient temperature of the microwave rain gauge, there are a multitude of choices. Many different ICs have been manufactured to measure temperature. The varieties include different levels of accuracy, as well as, different ways of communicating with a microcontroller. A device that provides a nice balance of accuracy and cost is the TMP36, shown in Figure 45. The TMP36 is specified for ± 2 ℃ over the entire temperature spectrum of -40 to $+125$ ℃ and is ± 1 ℃ accurate at 25 ℃ with no calibration (Analog Devices, Inc., 2010). The low output impedance of the TMP36 and its linear output and precise calibration simplify interfacing it to an ADC.

The output of the device provides a 750 mV output at 25 ℃ and has an output scale of 10 mV/℃. The device can run off 2.7 to 5.5 V supply and is not ratiometric with the supply voltage. Since the device will be operating near a K-band radar, RF pickup is of a concern, as the TMP36 operates on very little supply current (<50 μA). To minimize the effects of radio frequency interference, it is suggested to place a 2.2 μF tantalum capacitor and a 0.1 μF capacitor as decoupling capacitors.

Figure 45. Photograph of the TMP36. The TMP36 is used to determine the ambient temperature for Doppler frequency correction over temperature.

The output of the TMP36 is fed to an ADC on the ATmega128 where a reading is made every time the microcontroller is about to serially communicate its information. The ADC reading is then manipulated, knowing that 500 mV equal 0 ℃ and the scale is 10 mV/℃, and output to the end user over serial communication.

CHAPTER VII

CONCLUSION

A microwave rain gauge sensor was explored and prototypes developed for use by hydrologists and other researchers. The sensor makes use of a Doppler sensor module that outputs a Doppler frequency that is equivalent to the velocity of a target, in this case falling rain droplets. Through an analog signal processing chain, the Doppler sensor module's output is filtered, amplified, non-linearly amplified and digitized. The digitization of the signal allows for a microcontroller to properly interpret the signal. Since the temperature of the device and the angle of operation of the device affect the output of the Doppler sensor, a temperature sensor and accelerometer were included in the design to monitor these two parameters, respectively. The microcontroller then outputs the collected data through a serial port at a user specified time rate. Providing serial communication allows for a simplified process for connecting to data loggers, computers and other devices to view the data.

Future Work

Although the prototyped boards, shown in Figure 46, showed signs of success, there are still upgrades that could be made. The device still struggles with the S/N ratio of small drops at distances greater than 0.5 m away and, consequently, the device's output will be more heavily weighted towards large drops within the same area of observation. Possible solutions include going to more elaborate filtering schemes to reduce the noise, developing an algorithm that ignores large drops in regions where small drops cannot be detected or a combination of both. Another option that will help alleviate noise in the system is having a high quality PCB layout. With proper placement of ICs, components, ground planes etc., the possible noise interjected into the system is lessened.

Besides creating a final, high quality PCB, a watertight housing must be developed to house the electronics. The housing is equally as important as the electronics design in order to call the system successful. When a complete system is developed and field ready, extensive field trials must be conducted in order to determine the ability of the developed microwave rain gauge to accurately measure rainfall rates. If possible, the field trials should include a co-located tipping bucket rain gauge and a DICKEY-john Radar I. This will allow for comparison to a well accepted rain gauge in the tipping bucket and a direct comparison to a device capable of similar measuring techniques in the DICKEY-john Radar I.

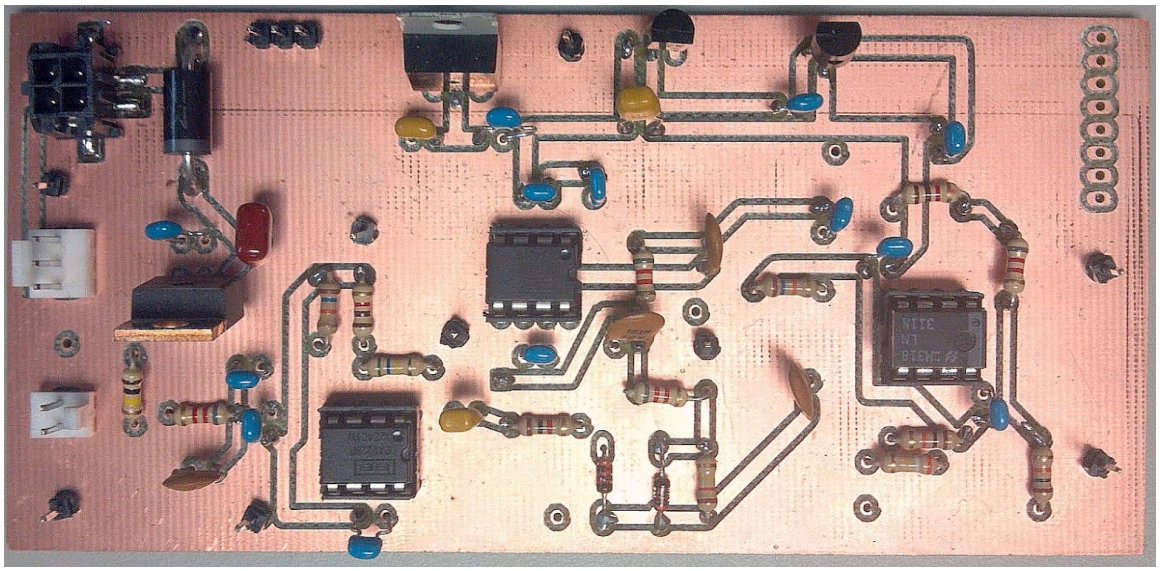

Figure 46. Photograph of one of the prototype boards developed.

APPENDIX A

IEEE RADIO SPECTRUM BANDS

Table A1. IEEE Radio Spectrum Bands

Band	**Wavelength (cm)**	**Frequency Range (GHz)**	**Origin of name**
HF	1,000-10,000	0.003-0.03	**H**igh **F**requency
VHF	100-1,000	0.03-0.3	**V**ery **H**igh **F**requency
UHF	30-100	0.3-1	**U**ltra **H**igh **F**requency
L	15-30	1-2	**L**ong wave
S	8-15	2-4	**S**hort wave
C	4-8	4-8	**C**ompromise between S and X
X	2.5-4	8-12	
Ku	1.7-2.5	12-18	**K**urz-**u**nder
K	1.1-1.7	18-27	**K**urz
Ka	0.75-1.1	27-40	**K**urz-**a**bove
V	0.4-0.75	40-75	
W	0.27-0.4	75-110	
Mm	0.1-0.27	110-300	

Source: IEEE Aerospace & Electronic Systems Society. (2003, January 8). IEEE Standard for Letter Designations for Radar-Frequency Bands. New York.

APPENDIX B

HORN ANTENNA TEMPLATE

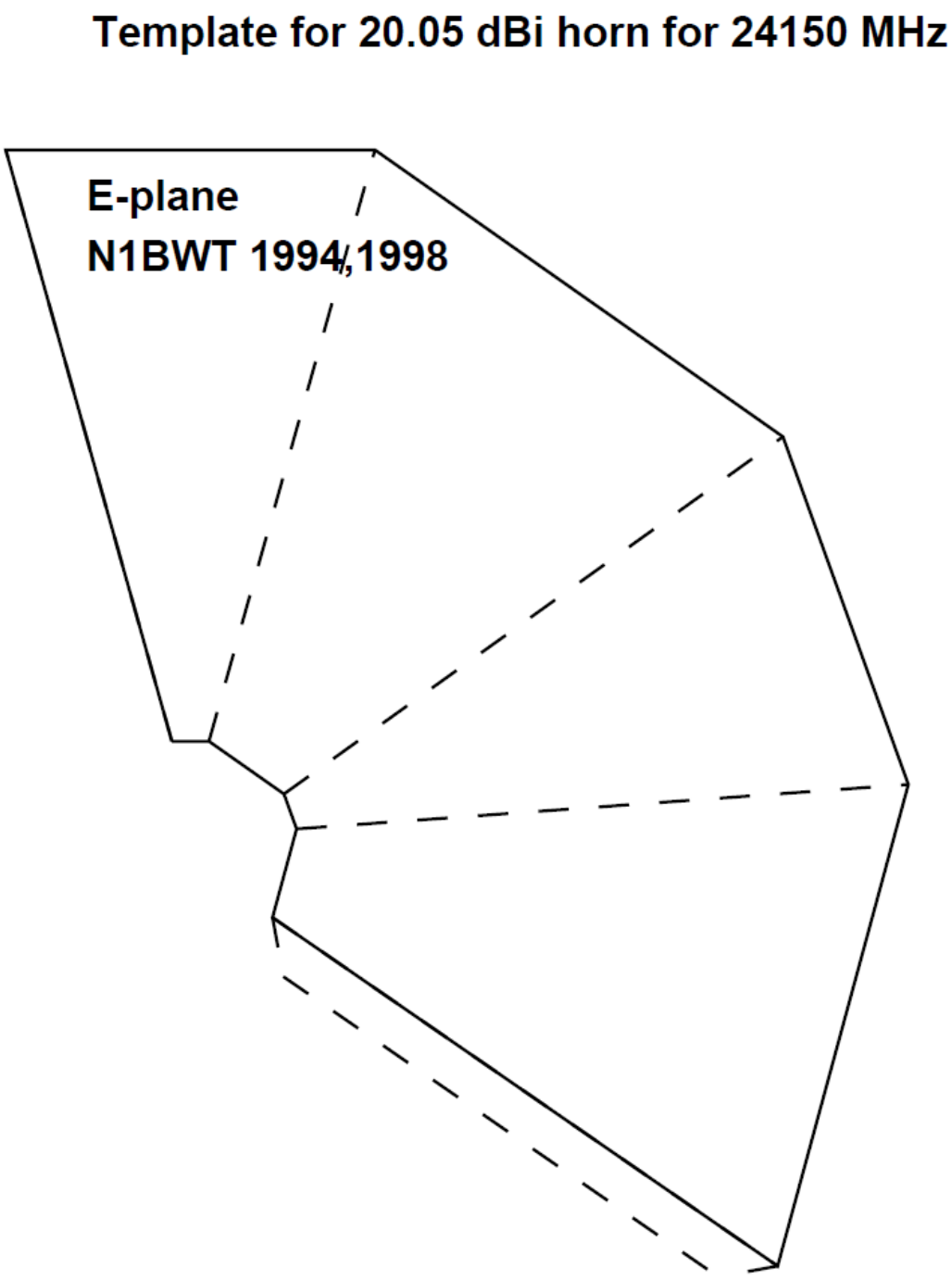

REFERENCES

Analog Devices, Inc. (2009). *ADXL335*. Retrieved February 2012, from Sparkfun Electronics: http://www.sparkfun.com/datasheets/Components/SMD/adxl335.pdf

Analog Devices, Inc. (2010). *TMP36*. Retrieved February 16, 2012, from Analog Devices: http://www.analog.com/static/imported-files/data_sheets/TMP35_36_37.pdf

Atlas, D., Srivastava, R. C., & Sekhon, R. S. (1973). Doppler characteristics of precipitation at vertical incidence. *Reviews of Geophysics and Space Physics, 11*(1), 1-35.

Atmel Coporation. (2011). *doc2467*. Retrieved February 10, 2012, from Atmel: http://www.atmel.com/Images/doc2467.pdf

Balanis, C. A. (2005). *Antenna Theory: Analysis and Design* (3rd ed.). Hoboken: John Wiley & Sons, Inc.

Caracciolo, C., Natali, S., Prodi, F., & Tagliavini, A. (2002). *Poster EGS 2002*. Retrieved March 9, 2012, from Nubila.

Digi International Inc. (2008). *Fox (LP3500) User's Manual.* Retrieved February 2012, from Digi: http://ftp1.digi.com/support/documentation/0190111_l.pdf

DISTROMET LTD. (n.d.). Retrieved March 8, 2012, from NOAA Earth System Research Laboratory: http://www.esrl.noaa.gov/psd/data/obs/instruments/ImpactDisdrometer.pdf

Franco, S. (2002). *Design with Operational Amplifiers and Analog Integrated Circuits* (3rd ed.). New York: McGraw-Hill.

Halliday, D., Resnick, R., & Walker, J. (2008). *Fundamentals of Physics* (Vol. I). Danvers: John Wiley & Sons, Inc.

IEEE Aerospace & Electronic Systems Society. (2003, January 8). IEEE Standard for Letter Designations for Radar-Frequency Bands. New York.

Krajewski, W. F., Kruger, A., Caracciolo, C., Gole, P., Barthes, L., Creutin, . . . Vinson, J.-P. (2006, February). DEVEX-disdrometer evaluation experiment: Basic results and implications for hydrologic studies. *Advances in Water Resources, 29*(2), 311-325.

Kruger, A., & Witold, K. (2002). Two-dimensional video disdrometer: A description. *Journal of Atmospheric and Oceanic Technology, 19*, 602.

Malik, N. R. (1995). *Electronic Circuits : Analysis, Simulation, and Design.* Englewood Cliffs: Prentice-Hall, Inc.

Mansheim, T. J., Kruger, A., Niemeir, J., & Brysiewicz, A. J. (2010). A Robust Microwave Rain Gauge. *IEEE Transactions on Instrumentation and Measurement*, 2204-2210.

National Semiconductor Corporation. (1969, March). *High Q Notch Filter.* Retrieved February 2012, from National: http://www.national.com/ms/LB/LB-5.pdf

Neamen, D. A. (2007). *Microelectronics Circuit Analysis and Design Third Edition.* New York: The McGraw-Hill Companies, Inc.

Rinehart, R. E. (2004). *Radar for Meteorologists Fourth Edition.* Nevada, MO: Rinehart Publications.

Skolnik, M. (2003). *Introduction to Radar Systems* (3rd ed.). McGraw-Hill Education (India) Pvt Ltd.